NFE2L3 Controls Colon Cancer Cell Growth through Regulation of DUX4, a CDK1 Inhibitor

Bury, Marina; Le Calve, Benjamin; Lessard, Frédéric; Dal Maso, Thomas; Saliba, James; Michiels, Carine; Febeyre, Gerardo; Vloker, Blank

Published in:
Cell Reports

DOI:
10.1016/j.celrep.2019.09.087

Publication date:
2019

Document Version
Publisher's PDF, also known as Version of record

Article

Cell Reports

NFE2L3 Controls Colon Cancer Cell Growth through Regulation of DUX4, a CDK1 Inhibitor

Graphical Abstract

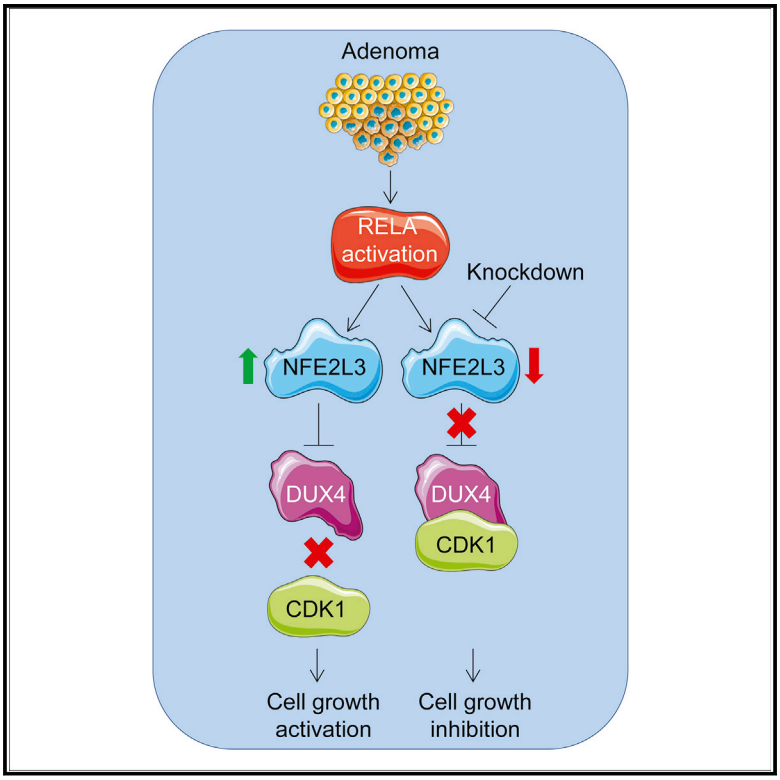

Authors

Marina Bury, Benjamin Le Calvé, Frédéric Lessard, ..., Carine Michiels, Gerardo Ferbeyre, Volker Blank

Correspondence

volker.blank@mcgill.ca

In Brief

Bury et al. show that the expression of the transcription factor NFE2L3 is regulated by NF-κB and that NFE2L3 levels are elevated in colon cancer patients. Knockdown of NFE2L3 inhibits colon cancer cell proliferation through induction of DUX4, a direct inhibitor of CDK1, establishing a pathway governing colon tumor growth.

Highlights

- NFE2L3 levels are elevated in colon cancer patients
- NFE2L3 expression is regulated by the RELA subunit of NF-κB
- Silencing of NFE2L3 decreases colon cancer cell proliferation
- NFE2L3 acts as a repressor of DUX4, a direct inhibitor of CDK1 activity

Bury et al., 2019, Cell Reports *29*, 1469–1481
November 5, 2019
https://doi.org/10.1016/j.celrep.2019.09.087

CellPress

Cell Reports
Article

NFE2L3 Controls Colon Cancer Cell Growth through Regulation of DUX4, a CDK1 Inhibitor

Marina Bury,[1,7,9] Benjamin Le Calvé,[4,8,9] Frédéric Lessard,[4] Thomas Dal Maso,[5] James Saliba,[1] Carine Michiels,[6] Gerardo Ferbeyre,[4] and Volker Blank[1,2,3,10,*]

[1]Lady Davis Institute for Medical Research, McGill University, Montreal, QC H3T 1E2, Canada
[2]Department of Medicine, McGill University, Montreal, QC H3T 1E2, Canada
[3]Department of Physiology, McGill University, Montreal, QC H3T 1E2, Canada
[4]Department of Biochemistry, University of Montreal, Montreal, QC H3C 3J7, Canada
[5]Department of Chemistry, Namur Medicine and Drug Innovation Center (NAMEDIC-NARILIS), University of Namur, 5000 Namur, Belgium
[6]URBC-NARILIS, University of Namur, 5000 Namur, Belgium
[7]Present address: De Duve Institute, UCLouvain, 1200 Brussels, Belgium
[8]Present address: URBC-NARILIS, University of Namur, 5000 Namur, Belgium
[9]These authors contributed equally
[10]Lead Contact
*Correspondence: volker.blank@mcgill.ca
https://doi.org/10.1016/j.celrep.2019.09.087

SUMMARY

Constitutive nuclear factor κB (NF-κB) activation is a hallmark of colon tumor growth. Cyclin-dependent kinases (CDKs) are critical cell-cycle regulators, and inhibition of CDK activity has been used successfully as anticancer therapy. Here, we show that the NFE2L3 transcription factor functions as a key regulator in a pathway that links NF-κB signaling to the control of CDK1 activity, thereby driving colon cancer cell proliferation. We found that NFE2L3 expression is regulated by the RELA subunit of NF-κB and that NFE2L3 levels are elevated in patients with colon adenocarcinoma when compared with normal adjacent tissue. Silencing of NFE2L3 significantly decreases colon cancer cell proliferation *in vitro* and tumor growth *in vivo*. NFE2L3 knockdown results in increased levels of double homeobox factor 4 (DUX4), which functions as a direct inhibitor of CDK1. The discovered oncogenic pathway governing cell-cycle progression may open up unique avenues for precision cancer therapy.

INTRODUCTION

Dysfunctional transcriptional and signaling networks have a fundamental role in colorectal cancer (CRC), one of the most common and fatal malignancies worldwide (Kuipers et al., 2015). Different molecular CRC subtypes have been identified, and understanding of the underlying pathogenesis of CRC formation is crucial for predicting prognosis and treatment response (De Sousa E Melo et al., 2013). The formation of CRC includes hereditary elements, but, in most cases, is sporadic and forms gradually over several years through the adenoma-carcinoma sequence. Mutations in *APC*, *KRAS*, and *TP53*, in conjunction with chromosomal instability, have been implicated in CRC development; nevertheless, other pathways can drive tumorigenesis as well (Brenner et al., 2014; Cancer Genome Atlas Network, 2012). Activation of the nuclear factor κB (NF-κB) transcription factor has a critical role in many cancer processes, including inflammation, growth, angiogenesis, invasion, metastasis, and resistance (Aggarwal and Sung, 2011). In addition, NF-κB is involved in the initiation and progression of CRC (Karin et al., 2002; Vaiopoulos et al., 2013). Multiple pathways associated with uncontrolled cell proliferation, including phosphatidylinositol 3-kinase (PI3K)-AKT-mechanistic target of rapamycin (mTOR), have been linked to NF-κB signaling (Dan et al., 2008). NF-κB also controls the levels of key cell-cycle regulators, such as cyclin D1, MYC, and cyclin-dependent kinases (CDKs) (Hinz et al., 1999; Karin et al., 2002; La Rosa et al., 1994; Perkins et al., 1997). Overexpression of NF-κB strongly correlates with worse overall survival of CRC patients (Wu et al., 2015). Moreover, increased levels of tumor necrosis factor (TNF), a cytokine inducing NF-κB activity, have been associated with advanced stages of CRC (Al Obeed et al., 2014), and chronic TNF exposure contributes to a pro-malignant phenotype (Szlosarek et al., 2006).

Cap'n'collar (CNC) transcription factors have crucial roles in a variety of cellular processes, including the stress response and carcinogenesis, with its most extensively investigated family member being the NFE2L2 (NRF2) protein (DeNicola et al., 2011). NFE2L3 (NRF3), a close homolog of NFE2L2, is less well studied and its functions remain largely unknown (Chevillard and Blank, 2011), but some recent findings linked the transcription factor to apoptosis and different types of cancer (Chowdhury et al., 2017; Siegenthaler et al., 2018; Sun et al., 2019; Wang et al., 2017, 2018). Similar to other CNC proteins, NFE2L3 dimerizes with small MAF transcription factors, and the resulting complexes bind to the antioxidant response element (ARE) type of DNA-recognition sites (Chénais et al., 2005). NFE2L3 transcript and protein levels are induced by TNF (Chénais et al., 2005). NFE2L3 is a tightly regulated and post-translational-modified protein with a rapid turnover (Nouhi et al., 2007), and FBXW7 ubiquitin ligase and GSK3B have

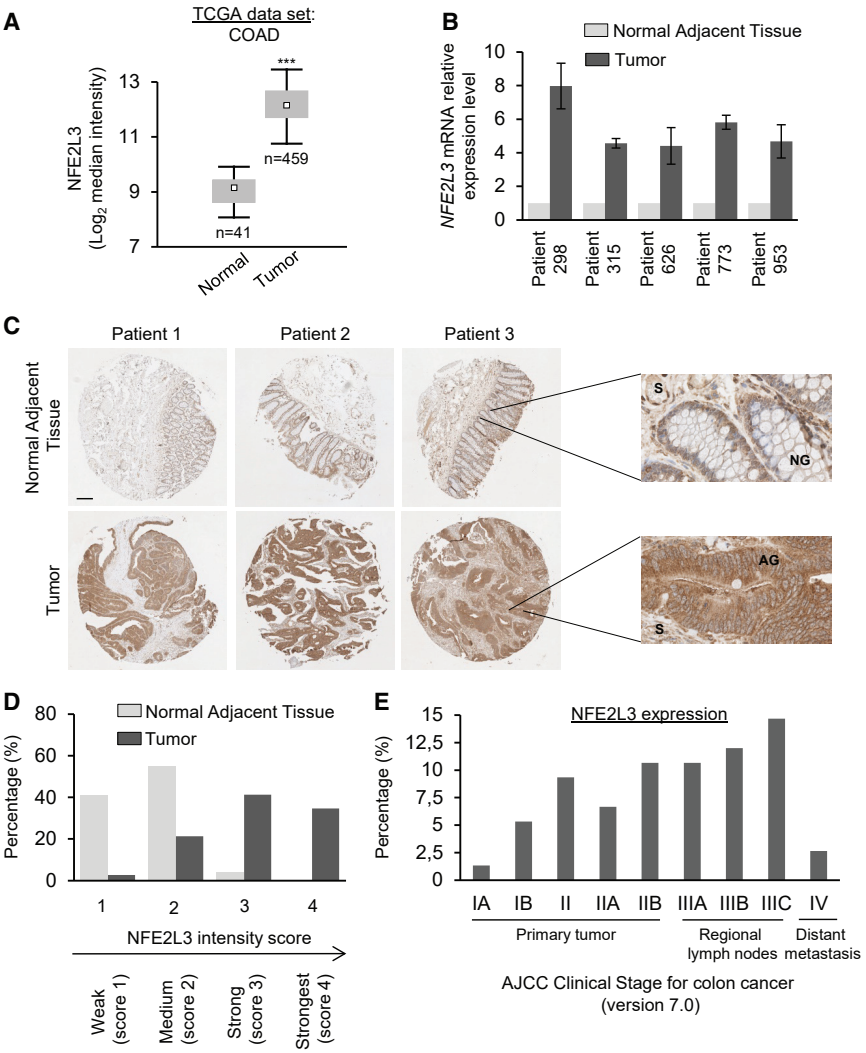

Figure 1. Upregulation of NFE2L3 Correlates with Poor Prognosis for Patients with Colon Cancer

(A) Colon adenocarcinoma (COAD) cancer gene expression data (mRNA, normalized RNA-seqV2 RSEM) were retrieved from TCGA database using the cBioPortal for cancer genomics. Boxplots represent the first and third quartiles and median values; whiskers represent the 5th and 95th percentiles; Mann-Whitney U test, ***$p < 0.001$.

(B) Quantitative real-time PCR analysis of NFE2L3 expression in colon cancer tissues and the adjacent counterpart from five patients with colon adenocarcinoma (means ± SD).

(C) Representative IHC images of human colon adenocarcinoma TMA stained for NFE2L3. The scale bar represents 200 μm; on the right side, magnification ×80; S, stroma; NG, normal gland; AG, adenocarcinoma gland.

(D) Classification and quantification of samples according to the intensity of staining of NFE2L3 expression (n = 75).

(E) Distribution of the higher NFE2L3 expression tumor samples (score 3 and 4) using the AJCC Clinical Stage for Colorectal Cancer (Singh, 2017).

been shown to control NFE2L3 degradation (Kannan et al., 2015). Subcellular fractionation experiments revealed the presence of three forms of NFE2L3: a primarily endoplasmic reticulum (ER)-bound N-glycosylated A form, a cytoplasmic non-glycosylated B form, and a faster migrating, largely nuclear C form (Kannan et al., 2015; Nouhi et al., 2007). In this study, we aimed to unravel the cellular network governing NFE2L3 regulation and function. We report that NFE2L3 acts as a central player in an identified NF-κB signaling pathway that controls colon cancer cell growth.

RESULTS

NFE2L3 Controls Colon Tumor Growth

We investigated the mRNA levels of the NFE2L3 transcription factor in normal and tumoral tissues using The Cancer Genome Atlas (TCGA) database (Figure 1A). *NFE2L3* transcripts were significantly upregulated in colon adenocarcinoma (n = 459) compared with normal samples (n = 41). Similar results were observed in BioGPS and Oncomine datasets (Figure S1) as well as upon analysis of *NFE2L3* mRNA levels in a set of five colon adenocarcinomas and normal adjacent tissues by quantitative real-time PCR (Figure 1B). To evaluate NFE2L3 protein levels, we performed immunohistochemistry (IHC) staining on a tissue microarray (TMA) of 75 patients, revealing greater expression of NFE2L3 in colon adenocarcinoma compared with matched normal adjacent tissue (Figure 1C). We classified the samples into four groups with increasing staining intensity from weakest (score 1) to strongest (score 4) (Figure 1D). We observed that NFE2L3 expression was weak, falling into groups 1 and 2 in most adjacent normal tissues (95%). In contrast, NFE2L3 levels were high, falling into groups 2–4 in most colon tumor tissues (97%; Figure 1D). In colon adenocarcinoma glands, we observed a strong nuclear and strong rimmed perinuclear pattern for NFE2L3, which diffuses across their cytoplasm, whereas, in normal glands, the staining is mostly perinuclear and cytoplasmic (Figure 1C). We also found that the high expression of NFE2L3 in tumor samples is correlated with the advanced stages of the disease, except for the metastasis stage (Figure 1E). Together, these results suggest that NFE2L3 might have a critical role in colon adenocarcinoma development and may be linked to major oncogenic pathways.

Silencing NFE2L3 Inhibits Colon Cancer Cell Proliferation

To assess the role of NFE2L3 in colon cancer, we depleted NFE2L3 expression with two different lentiviral short hairpin RNAs (shRNAs) in distinct colon cancer cell lines HCT116 and HT29. Efficient knockdown of NFE2L3 was confirmed by quantitative real-time PCR and immunoblot (Figures 2A and 2B) and

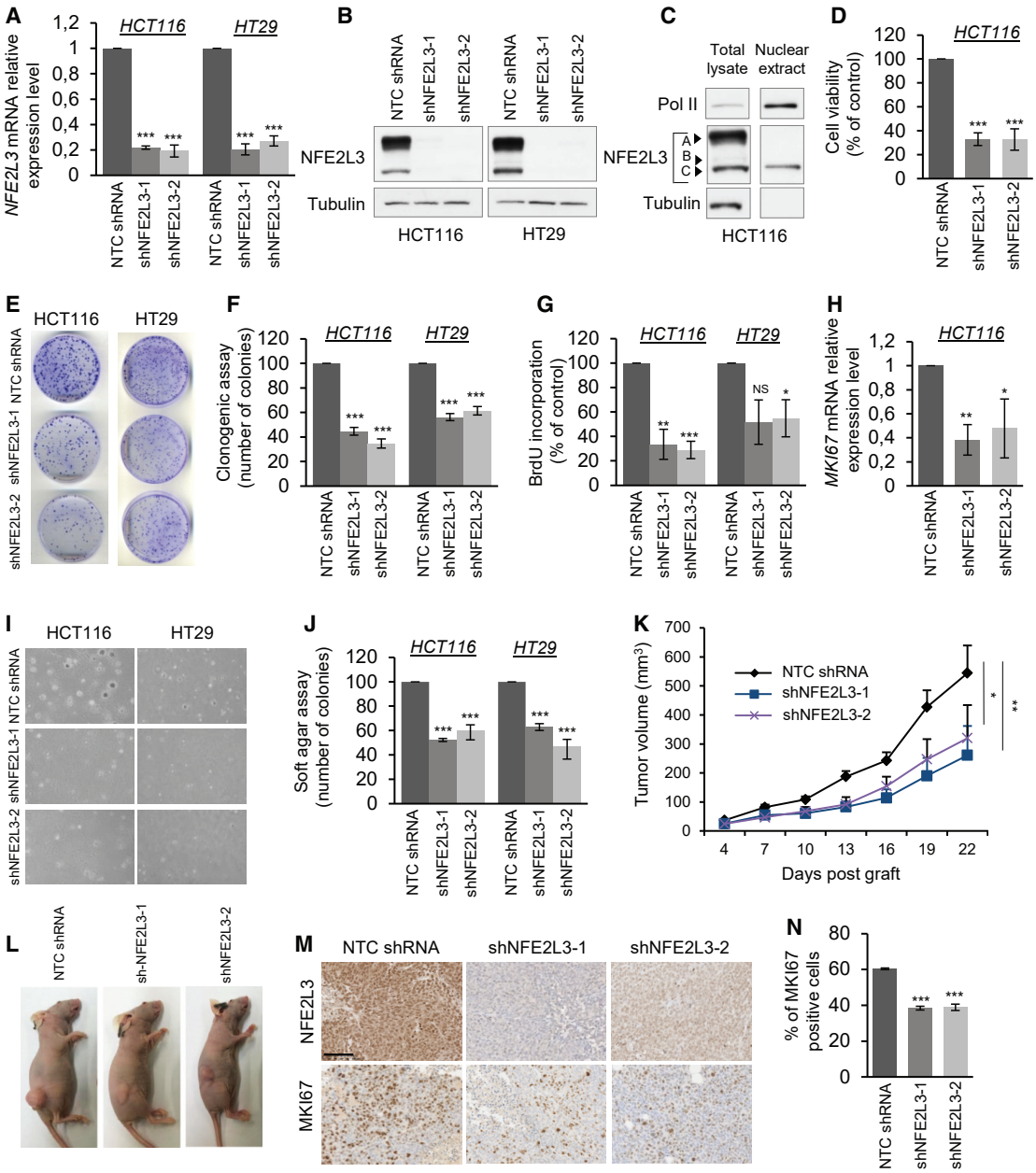

Figure 2. NFE2L3 Is Required for Colon Cancer Cell Growth *In Vitro* and *In Vivo*

(A) Quantitative real-time PCR analysis of *NFE2L3* mRNA in HCT116 and HT29 cells transduced with NFE2L3-specific shRNAs (shNFE2L3-1 or -2) presented relative to *NFE2L3* mRNA expression in cells transduced with a non-targeting control (NTC) shRNA.

(B) Immunoblot analyses of NFE2L3 in the cells described in (A).

(C) Immunoblot analyses of NFE2L3 from total lysate or nuclear extraction in HCT116 cells. Arrows indicate the A, B, and C form of NFE2L3.

(D) Cell viability in HCT116 cells assessed by MTT assay after 72 h. Error bars are means ± SEM, n = 3 independent experiments, ***p < 0.001, two-sided Student's t test.

(E and F) Representative images (E) and quantification (F) of a colony-formation assay of the HCT116 and HT29 cells. For each cell line, all dishes were fixed at the same time, stained, and photographed. Error bars are means ± SEM, n = 3 independent experiments, ***p < 0.001, two-sided Student's t test.

(G) Incorporation of BrdU in HCT116 and HT29 cells as measured by ELISA after treatment for 16 h. Error bars are means ± SEM, n = 3 independent experiments, *p < 0.05, **p < 0.01, ***p < 0.001, NS, not significant; two-sided Student's t test.

(H) Quantitative real-time PCR analysis of *MKI67* mRNA in HCT116 cells. Error bars are means ± SEM, n = 3 independent experiments, *p < 0.05, **p < 0.01, two-sided Student's t test.

(I and J) Representative images (I) and quantification (J) of HCT116 and HT29 cells by soft agar assay. Error bars are means ± SEM, n = 3 independent experiments, ***p < 0.001, two-sided Student's t test.

(legend continued on next page)

affected the abundance of all three previously characterized NFE2L3 A, B, and C forms (Figure 2C) (Nouhi et al., 2007). We observed a strong reduction in cell numbers three days after plating when NFE2L3 was knocked down, and colony formation was significantly reduced (Figures 2D–2F). No changes in apoptosis were observed by flow cytometry using Annexin V and propidium iodide (PI) staining (Figure S2). In contrast, reduced numbers of bromodeoxyuridine (BrdU)-incorporating cells, as well as a decrease in the mRNA expression of the *MKI67* (*Ki67*) gene coding for a major cell-proliferation marker, showed that NFE2L3 functions as a positive regulator of colon cancer cell growth (Figures 2G and 2H). To model physiological conditions, we evaluated anchorage-independent colon cancer cell growth in a soft agar assay (Figures 2I and 2J) and proliferation of HCT116 cells *in vivo* in a mouse xenograft model (Figure 2K and 2L). In both settings, NFE2L3 knockdown severely compromised cell growth. Reduced MKI67 staining in xenografts of NFE2L3 knockdown samples confirmed that this effect was largely due to reduced cell proliferation *in vivo* (Figures 2M and 2N). Altogether, these results establish a crucial role for NFE2L3 as a promoter of colon cancer cell proliferation and tumor growth.

RELA Functions as a Positive Regulator of NFE2L3 Expression

Our previous studies had shown that TNF increases NFE2L3 levels (Chénais et al., 2005). To determine the molecular mechanisms underlying NFE2L3 upregulation in colon cancer cells, we treated the cells with inhibitors of different signaling pathways upon TNF activation and assessed NFE2L3 levels. Specifically, we examined the effect of inhibiting the MEK1/2 (PD98059), p38 (SB203580), PI3K/AKT (LY294002), and NF-κB (BAY 11-7082) pathways because these signaling molecules have been previously linked to colon tumorigenesis (Karin, 2006; Cancer Genome Atlas Network, 2012). Although MEK1/2, p38, and PI3K/AKT inhibitors had no or minimal effect, we observed that the inhibitor of NF-κB signaling strongly reduced NFE2L3 levels (Figure 3A). NF-κB pathway is involved in inflammation, tumor survival, migration, and proliferation of colon cancer cells (Ben-Neriah and Karin, 2011; Karin, 2006; Wang et al., 2009). *In vivo*, colorectal cancer cells are exposed to a variety of cytokines released from the tumor stroma, including known activators of NF-κB signaling, such as TNF, which enhances the growth of colon cancer cells by the activation of oncogenic pathways (Ben-Neriah and Karin, 2011; Wang et al., 2009). Treatment of colon cancer cell lines with TNF increased NFE2L3 protein levels; this effect was strongly diminished upon treatment of cells with two mechanistically different inhibitors of NF-κB signaling (Figures 3B and 3C): BAY 11-7082 blocks TNF-induced NFKBIA (IκBα) phosphorylation, and JSH-23 functions as an inhibitor of NF-κB transcriptional activity (Pierce et al., 1997; Shin et al., 2004). The NF-κB transcription factor family comprises homo- and heterodimeric complexes that are formed by the combination of five different subunits, including RELA (p65), RELB, REL, NFKB1 (p50), and NFKB2 (p52) (Karin, 2006; Vaiopoulos et al., 2010). We found that shRNA-mediated knockdown of RELA significantly decreased NFE2L3 mRNA and protein expression levels (Figures 3D, 3E, and S3A–S3C), recapitulating the reduced growth phenotype associated with NFE2L3 silencing (Figures 3F and 3G). In contrast, downregulation of the NF-κB subunits REL, RELB, NFKB1, or NFKB2 had no effect on NFE2L3 expression (Figure S3). Consistent with this, data from the ENCODE project consortium showed binding of the RELA subunit of NF-κB to the first intron of NFE2L3 (Figure S4A) (ENCODE Project Consortium, 2012), which we confirmed by chromatin immunoprecipitation (ChIP)-qPCR analyses and luciferase reporter assays (Figures 3H–3J). To assess whether low NFE2L3 levels contribute to the inhibition of proliferation observed upon silencing of RELA in colon cancer cell lines, we overexpressed the NFE2L3 full form (generating A, B, and C), the ER/cytoplasmic A–B forms, or the nuclear C form of NFE2L3 and found that both expression of the full or C form of NFE2L3, but not the A–B form, partially rescued the phenotype of reduced colon cancer cell growth upon RELA knockdown, as confirmed by BrdU incorporation (Figures S4B and S4C). We conclude that RELA positively regulates NFE2L3 expression and thus may contribute to its protumoral effects.

Identification of DUX4 as a Negatively Regulated Target of NFE2L3

To investigate the mechanistic link between NFE2L3 and cell proliferation, we searched for genes controlled by NFE2L3 that may mediate its effect on colon cancer cell proliferation. To identify transcriptional targets, we carried out ChIP-sequencing with NFE2L3-specific antiserum in TNF-treated HCT116 cells. Among the identified potential NFE2L3 target genes, the *DUX4* gene emerged as a highly interesting candidate because it had been previously linked to the cell cycle (Bosnakovski et al., 2008). In addition, *DUX4* ranked as the top gene to have its NFE2L3 peaks converge when combining both fold enrichment and distance to the transcription start site (TSS) (Figure 4A). The binding of NFE2L3 to the DUX4 locus was corroborated by ChIP-qPCR analysis (Figure 4B), and knockdown of NFE2L3 resulted in a significant increase in *DUX4* mRNA (Figure 4C) and protein levels (Figure 4D). Reintroduction of the full form and the nuclear C form of NFE2L3 by lentiviral transduction reduced DUX4 levels and partially rescued cellular proliferation (Figures 4E and 4F). Consistent with these data, inhibition of NF-κB by RELA-knockdown or JSH-23 inhibitor treatment reduced NFE2L3 and increased DUX4 protein levels (Figures 4G and 4H). Thus, DUX4 is repressed by NFE2L3 and might have a role in the effects of NFE2L3 on cell proliferation. A gain-of-function phenotype of DUX4 has been linked to facioscapulohumeral muscular dystrophy (FSHD) (Bosnakovski et al., 2008; Gabellini

(K and L) Representative gross images (K) of the xenograft tumors at the endpoint and growth curves (L) of xenograft tumors derived from subcutaneously implanted HCT116 cells expressing a NTC shRNA or NFE2L3-specific shRNAs (shNFE2L3-1 or -2). Error bars are means ± SEM, n=9 mice per group, *p<0.05, **p<0.01, Mann-Whitney U test.

(M) Representative images of NFE2L3 and MKI67 analyzed by immunohistochemical staining.

(N) Quantification of MKI67 analyzed by immunohistochemical staining. The scale bar represents 100 μm. The bar graph shows the percentage of MKI67-positive cells. Error bars are means ± SEM, n = 3 mice per group, ***p < 0.01, two-sided Student's t test.

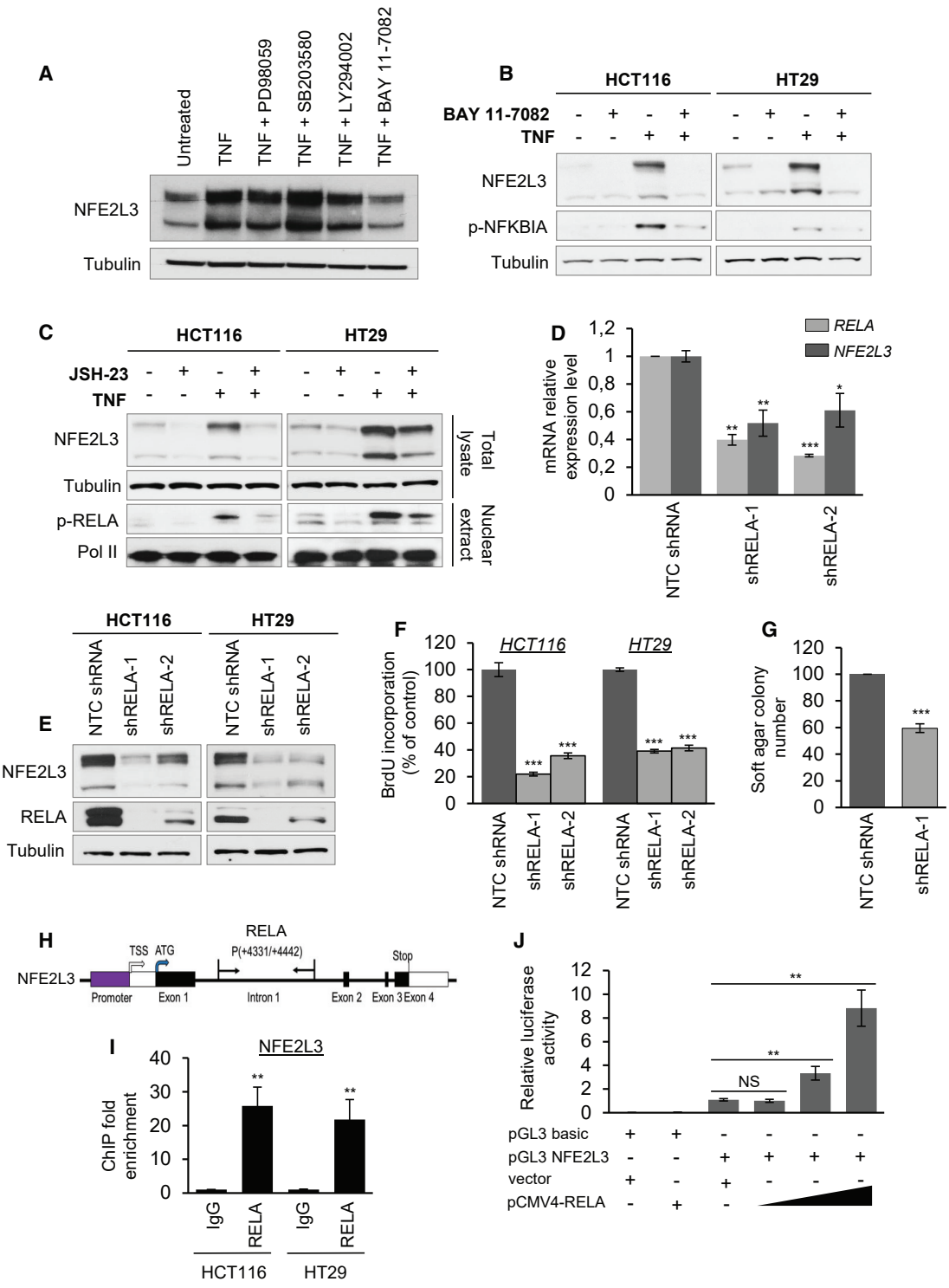

Figure 3. NFE2L3 Is Regulated by the RELA Subunit of NF-κB

(A) HCT116 cells were pretreated with PD98059 (20 μM), SB203580 (20 μM), LY294002 (20 μM), and BAY 11-7082 (10 μM) for 2 h, followed by stimulation with TNF (20 ng/mL) for 6 h. The expression of NFE2L3 was examined by immunoblot.

(B) Immunoblot analysis of NFE2L3 in HCT116 and HT29 cells pretreated with BAY 11-7082 (10 μM, 2 h) followed by stimulation with TNF (20 ng/mL, 6 h).

(C) Immunoblot analysis of NFE2L3 in HCT116 and HT29 cells pretreated with JSH-23 (50 μM, 16 h) followed by stimulation with TNF (20 ng/mL, 6 h).

(legend continued on next page)

et al., 2002), but its function in cancer remains unclear, despite some recent data showing that DUX4 is deregulated in acute lymphoblastic leukemia and can control the migration of mesenchymal stem cells (Dmitriev et al., 2016; Yasuda et al., 2016; Zhang et al., 2016). We found that lentiviral overexpression of DUX4, driven by a strong (cytomegalovirus [CMV]), as well as weak, promoter (ubiquitin C [UBC]), is toxic and leads to the death of most cells within 24–48 h (data not shown). To assess whether elevated DUX4 levels contribute to the inhibition of proliferation observed upon silencing of NFE2L3 in colon cancer cell lines, we thus knocked down DUX4 and observed that combined NFE2L3 and DUX4 depletion partially rescued the phenotype of reduced colon cancer cell growth, as confirmed by BrdU incorporation and soft agar assays (Figures 4I–4L). We also analyzed *DUX4* mRNA levels in colon adenocarcinomas and normal adjacent tissue specimens. We found decreased DUX4 transcript levels in four of the five colon adenocarcinomas samples, thus correlating well with NFE2L3 expression (Figures 1B and S5A). Overall, these data suggest that DUX4 mediates in part the proliferation phenotype observed upon modulation of RELA and/or NFE2L3 levels.

Role of DUX4 as a Direct Inhibitor of CDK1 Activity

To understand how DUX4 might affect cell proliferation, we searched for DUX4-interacting proteins in colon cancer cells by performing immunoprecipitation followed by mass spectrometry analysis in HCT116 cells. Using ReactomePA (Yu and He, 2016), we identified different cell-cycle regulators, including cyclin-dependent kinase 1 (CDK1), as potential binding partners for DUX4, providing a rationale for the role of NFE2L3 in the control of colon cancer cell proliferation (Figure S5B; Table S1). We confirmed the interaction between DUX4 and CDK1 by co-immunoprecipitation of epitope-tagged CDK1 and DUX4 co-expressed in HCT116 cells (Figure 5A). In parallel, we performed co-immunoprecipitation experiments with three additional CDKs (CDK2, 4, and 6) to verify the specificity of the DUX4-CDK1 interaction (Figure 5A). Clearly, interaction between DUX4 and CDK1 is stronger than that with other members of the CDK family. Immunoprecipitation of endogenous CDK1 from cells expressing NFE2L3 shRNA, which increases endogenous DUX4 protein levels, confirmed the interaction between this kinase and the DUX4 protein (Figure 5B). Furthermore, we designed an *in silico* model of the DUX4-CDK1 complex using the ZDOCK server (Figures 5C, 5D, and S6A). Based on the complex CDK1-cyclin B1-CKS2 available on the PDB, we separated the three proteins to generate a model for DUX4-CDK1 interactions. The model predicts that DUX4 binds CDK1 at the same location as CDC28 protein kinase regulatory subunit 2 (CKS2), and we identified the amino acids implicated in this binding (Brown et al., 2015) (Figure S6B). A series of interactions are involved in the formation of the complex, including hydrogen bonds and electrostatic as well as van der Waals interactions. We compared the sequences of CDK1 with CDK2, CDK4, and CDK6 to illustrate the variations among the different members of the CDK protein family and the difference of binding with DUX4. Our model suggests that the binding between DUX4 and CDK1 is mediated by a series of residues present in conserved domains of the CDK family but the variability of some amino acids may explain the difference of affinity observed in Figure 5A (Figure S6C). Based on these *in silico* models, we generated three different mutants to characterize the domain of DUX4 implicated in the interaction with CDK1 (Figure 5E). Deletion of amino acids from position 111–131 strongly, and deletion from position 141–180 moderately, reduced the interaction with CDK1, whereas deletion of aa 381–400 had no effect (Figure 5F). We investigated more precisely the amino acids implicated in the interaction between DUX4 and CDK1 (Figure S6B), and based on those predictions, we generated two mutants, Arg117Ala and Phe118Ala, of DUX4. By immunoprecipitation, we observed that the interaction between CDK1 and those DUX4 mutants is reduced compared with the wild-type form of the protein (Figure 5G). Next, we performed glutathione S-transferase (GST) pull-down comparing the binding of DUX4 to CDK1 and the CDK1-cyclin B complex (Figures 6A and 6B). Our data showed that DUX4 preferentially interacts directly with CDK1 alone and only minimally with the CDK1-cyclin B complex. In addition, we quantitatively assessed the interaction between DUX4-GST and CDK1-His tag by microscale thermophoresis (MST). We determined a K_D (dissociation constant) of 1.7 ± 0.1 μM for the binding of DUX4 to CDK1 (Figure 6C). GST alone was used as negative control. Together, our results show that the DUX4 protein directly interacts with CDK1.

To determine whether DUX4 inhibits the activity of CDK1, we immunoprecipitated CDK1 and assessed its *in vitro* kinase activity on recombinant histone H1 protein (Ruiz et al., 2010). We showed that CDK1 activity, measured by H1 phosphorylation, was strongly decreased in cells after NFE2L3 knockdown but was not altered in control cells, after a single DUX4 or a combined NFE2L3/DUX4 knockdown (Figure 6D). Cell-cycle profiling and high levels of NUP98 also showed that silencing of NFE2L3 leads to an accumulation of cells in the G2/M phase, which is controlled by the CDK1-cyclin B complex (Laurell et al., 2011)

(D) Quantitative real-time PCR analysis of *RELA* and *NFE2L3* mRNA in HCT116 cells transduced with a NTC shRNA or RELA-specific shRNAs (shRELA-1 or -2). Error bars are means ± SEM, n = 3 independent experiments, *p < 0.05, **p < 0.01, ***p < 0.001, two-sided Student's t test.
(E) Immunoblot analysis of RELA and NFE2L3 in HCT116 and HT29 cells transduced with a NTC shRNA or RELA-specific shRNAs (shRELA-1 or -2).
(F) BrdU incorporation measured by ELISA in HCT116 and HT29 cells transduced with a NTC shRNA or RELA-specific shRNAs (shRELA-1 or -2). Error bars are means ± SD, n = 2 independent experiments, ***p < 0.001, two-sided Student's t test.
(G) Quantification of soft agar assay of HCT116 cells transduced with a NTC shRNA or a RELA-specific shRNA (shRELA-1). Error bars are means ± SEM, n = 3 independent experiments, ***p < 0.001, two-sided Student's t test.
(H) Localization of a RELA binding site in the *NFE2L3* gene locus.
(I) ChIP analyses were performed in HCT116 and HT29 cells using anti-RELA antibody. An immunoglobulin G (IgG) antibody was used as negative control. Fold enrichment was quantified by qPCR. Error bars are means ± SEM, n = 3 independent experiments, **p < 0.01, two-sided Student's t test.
(J) Luciferase assay: 293T cells were transfected with the indicated plasmids. After incubation for 24 h, luciferase activity was measured and normalized to *Renilla*. Error bars are means ± SEM, n = 3 independent experiments, **p < 0.01, NS, not significant; two-sided Student's t test.

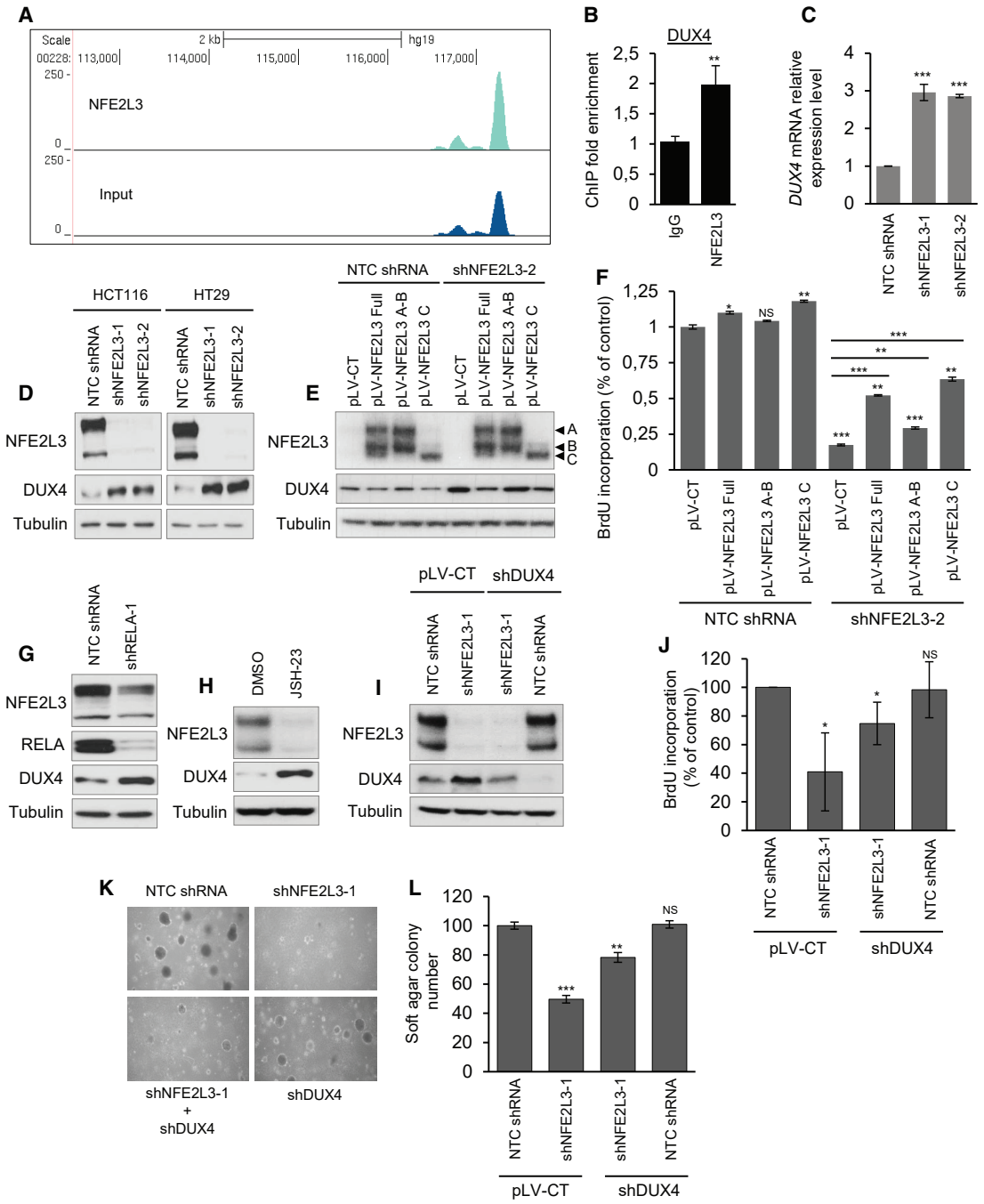

Figure 4. NFE2L3 Functions as a Repressor of DUX4

(A) Example of NFE2L3 ChIP-sequencing traces in HCT116 cells.

(B) ChIP-qPCR validation of NFE2L3 binding to the DUX4 locus using NFE2L3 or IgG control antibody. Error bars are means ± SEM, n = 3 independent experiments, $^{**}p < 0.01$, two-sided Student's t test.

(C) Expression of *DUX4* mRNA assayed by quantitative real-time PCR in HCT116 cells. Error bars are means ± SEM, n = 3 independent experiments, $^{***}p < 0.001$, two-sided Student's t test.

(D) Immunoblot analysis of NFE2L3, DUX4, and tubulin in HCT116 and HT29 cell lines transduced with a NTC shRNA or NFE2L3-specific shRNAs (shNFE2L3-1 or -2).

(E) Immunoblot analysis of HCT116 cells expressing NFE2L3 shRNA (shNFE2L3-2) or a NTC shRNA upon reexpression of the different forms of NFE2L3 (see Figure 2C for description of A, B, or C forms).

(legend continued on next page)

(Figures 6E–6G). The decrease of CDK1 activity might thus explain the reduced colon cancer cell proliferation upon knockdown of NFE2L3. In conclusion, our data reveal a link between the NF-κB signaling pathway and cell-cycle regulation, with NFE2L3 acting as a repressor of the CDK1 inhibitor DUX4 (Figure 6H).

DISCUSSION

Colorectal cancer ranks as the third most common cancer worldwide (Kuipers et al., 2015). The underlying molecular mechanisms of CRC pathology are complex, comprising a variety of genetic and epigenetic factors that control the proliferation rate of cells, their differentiation, and proneness to undergo cell death (Cancer Genome Atlas Network, 2012; Vinson et al., 2016). We found that NFE2L3 levels are substantially elevated in human colon adenocarcinoma tissue specimens when compared with healthy adjacent tissue, suggesting a possible role for this transcription factor in colon tumorigenesis. The signaling cascade discovered in our study comprises the extensively analyzed NF-κB and NFE2L3, a factor of yet largely unknown function. These transcriptional regulators are linked to the central cell cycle regulator CDK1, via the control of DUX4, a protein that has previously primarily been analyzed in the context of muscle biology (Chevillard and Blank, 2011; Gabellini et al., 2002; Zhang et al., 2017).

In our earlier studies, we reported that NFE2L3 expression is positively controlled by TNF at both the transcript and protein levels (Chénais et al., 2005). In addition, many studies have linked the NF-κB pathway to TNF signaling (Li et al., 2015). Our data identified NFE2L3 as a novel downstream effector of RELA, as we found that other NF-κB family members are not involved in the regulation of NFE2L3. As confirmed by ChIP analysis, the control of NFE2L3 transcription by NF-κB is direct. The regulation by RELA is robust because inhibition of the transcriptional activity of NF-κB, NFKBIA phosphorylation, or knockdown of RELA all recapitulated the phenotype observed upon NFE2L3 silencing. This is of interest because RELA is constitutively activated in human CRC tissue (Rezapour et al., 2016). Additional studies revealed that NOTCH1 levels, which were found to be an independent predictor of prognosis for patients with CRC, correlated with RELA status (Chu et al., 2011). NF-κB is also known to modulate Wnt signaling, whose activation is a common event in colon cancer initiation: ablation of RELA in intestinal epithelial cells delays the expansion of crypt stem cells, whereas elevated NF-κB signaling results in the dedifferentiation of non-stem cells into tumor-initiating cells (Schwitalla et al., 2013). These data illustrate the importance of RELA in CRC development. The identification of NFE2L3 as a RELA target provides novel avenues to dissect the functions of NF-κB signaling pathway in colon cancer pathology.

NFE2L3 has been first identified almost 20 years ago but its function remains largely unknown (Chevillard and Blank, 2011). Mouse model experiments revealed that NFE2L3 has a protective function in carcinogen-induced lymphomagenesis (Chevillard et al., 2011). Recent studies implicated NFE2L3 in various types of malignancies, including pancreatic, thyroid, and breast cancer (Sun et al., 2019; Wang et al., 2017, 2018). Our results demonstrate a growth-promoting function of NFE2L3 in colon cancer cells, which is likely mediated by the nuclear C form of the transcription factor. Our ChIP-seq analysis, together with molecular analyses, revealed that NFE2L3 serves as a key regulator for the control of DUX4 expression. The DUX4 protein has mainly been investigated for its role in FSHD. The *DUX4* gene, located in a transcriptionally silent repeat region, is present at high levels in FSHD muscle because of chromatin changes, contributing to the phenotype, but the exact mechanisms remain obscure (Eidahl et al., 2016). Of interest, DUX4 also contributes to leukemia and round-cell sarcoma because of somatic chromosomal rearrangements resulting in *DUX4-IGH* and *CIC-DUX4* fusions, respectively (Kawamura-Saito et al., 2006; Yasuda et al., 2016). Overexpression of DUX4 is toxic in many different cellular models and also results in increased sensitivity to oxidative stressors (Bosnakovski et al., 2008). Interestingly, in the context of colon cancer cells, upregulation of endogenous DUX4 protein upon NFE2L3 or RELA knockdown, results in a diminution of cell proliferation, but we did not observe any obvious toxicity to the cells, as measured by Annexin V/PI staining (Figure S2). However, overexpression of exogenous DUX4, even driven by a weak promoter, is highly toxic to the cells in our colon cancer cell model.

How is the function of NFE2L3 transcriptional regulator coupled to cell proliferation in our experimental model? Our studies revealed an unanticipated link, showing that DUX4 is able to interact with CDK1, a crucial cell-cycle regulator, as evidenced by immunoprecipitation, followed by mass spectrometry analysis. This result was confirmed by co-immunoprecipitation (coIP) studies of exogenous and endogenous proteins, by performing GST pull-down assays and by measuring the K_D of the interaction between DUX4 and CDK1, which is in the low micromolar range. *In silico* analysis highlighted amino acids potentially implicated in the interaction between DUX4 and CDK1, and based on these theoretical models,

(F) BrdU incorporation in HCT116 cells treated as in (E) assessed by ELISA. Error bars are means ± SEM, n = 3 independent experiments, *p < 0.05, **p < 0.01, ***p < 0.001, NS, not significant; two-sided Student's t test.
(G) Immunoblot analysis of NFE2L3, DUX4, and tubulin in HCT116 cells transduced with a NTC shRNA or a RELA-specific shRNA (shRELA-1).
(H) Immunoblot analysis of NFE2L3, DUX4, and tubulin in HCT116 cells treated with DMSO or JSH-23 (50 μM, 16 h).
(I) Immunoblot analysis of HCT116 cells transduced with a combination of vectors driving non-silencing controls (NTC shRNA or pLV scramble), shNFE2L3-1, or shDUX4.
(J) BrdU incorporation in HCT116 cells treated as in (I) assessed by ELISA. Error bars are means ± SEM, n = 3 independent experiments, *p < 0.05, NS, not significant; two-sided Student's t test.
(K and L) Representative images (K) of soft agar assay of HCT116 cells treated as in (I) and its quantification (L). Error bars are means ± SD, n = 2 independent experiments, **p < 0.01, ***p < 0.001, NS, not significant; two-sided Student's t test.

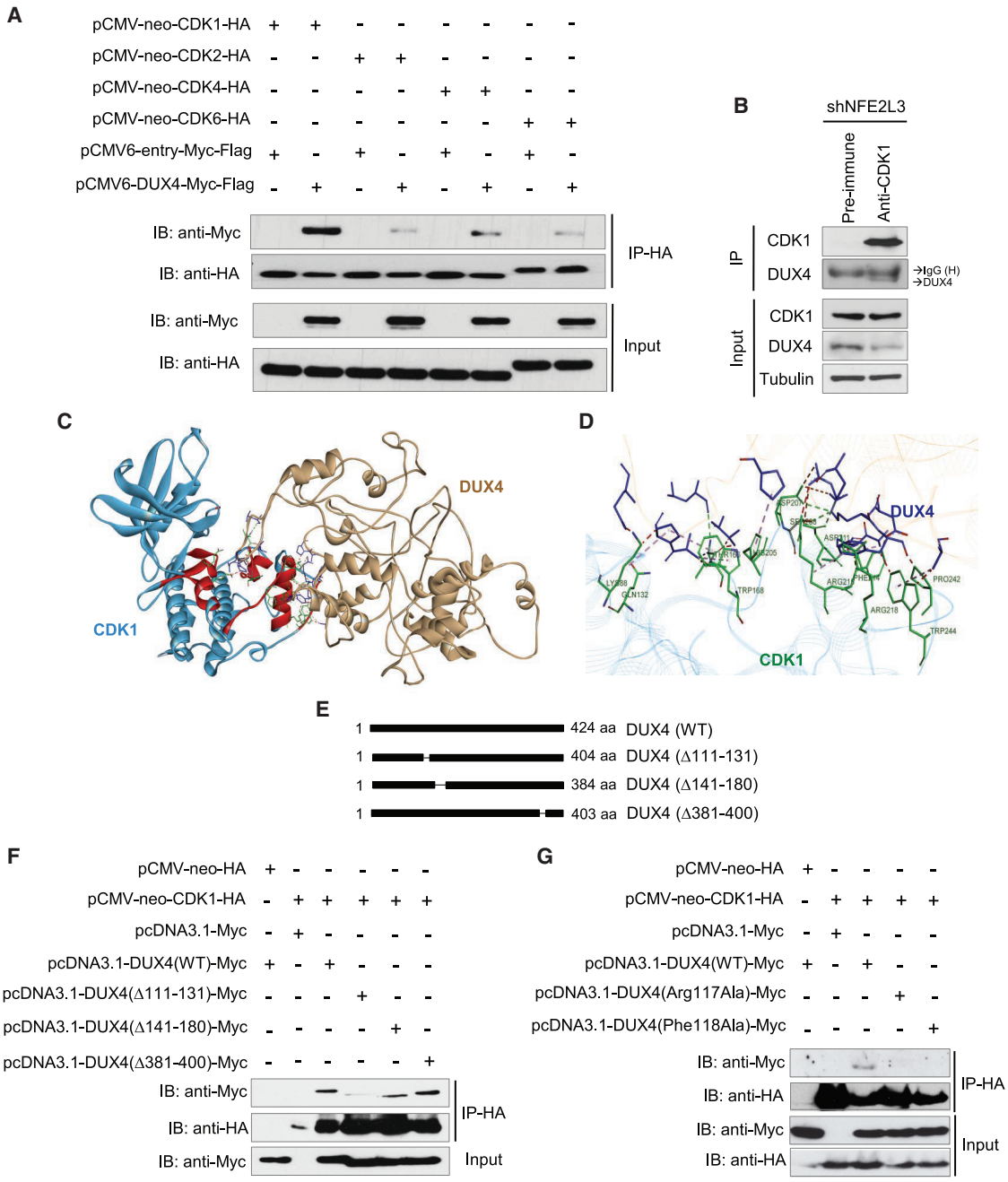

Figure 5. DUX4 Interacts with CDK1

(A) coIP of pCMV-neo-CDK1-HA, pCMV-neo-CDK2-HA, pCMV-neo-CDK4-HA, pCMV-neo-CDK6-HA, and pCMV6-entry-Myc-Flag or pCMV6-DUX4-Myc-Flag from HCT116-transfected cell lysates. Samples and lysates were analyzed by immunoblot.

(B) Immunoprecipitation of lysates from HCT116 cells transduced with shNFE2L3-1 using anti-CDK1 antibody. Samples and lysates were analyzed by immunoblot.

(C) Protein structure of the DUX4-CDK1 complex obtained with ZDOCK server. Amino acids implicated in the binding of DUX4 to CDK1 are highlighted and shown in detail in Figure S6B.

(D) DUX4-CDK1 interactions showing DUX4 (blue) and CDK1 (green) amino acids.

(E) Representation of the DUX4 mutants and their different regions.

(F) HCT116 cells were transiently transfected with vectors expressing HA-tag or CDK1-HA and Myc-tag, or DUX4(WT)-Myc, or DUX4(Δ111-131)-Myc, or DUX4(Δ141-180)-Myc, or DUX4(Δ381-400)-Myc. Proteins were immunoprecipitated with an anti-HA antibody, and samples were analyzed by immunoblotting.

(G) HCT116 cells were transiently transfected with vectors expressing HA-tag or CDK1-HA and Myc-tag, DUX4(WT)-Myc, DUX4(Arg117Ala)-Myc, or DUX4(Phe118Ala)-Myc. Proteins were immunoprecipitated with an anti-HA antibody, and samples were analyzed by immunoblotting.

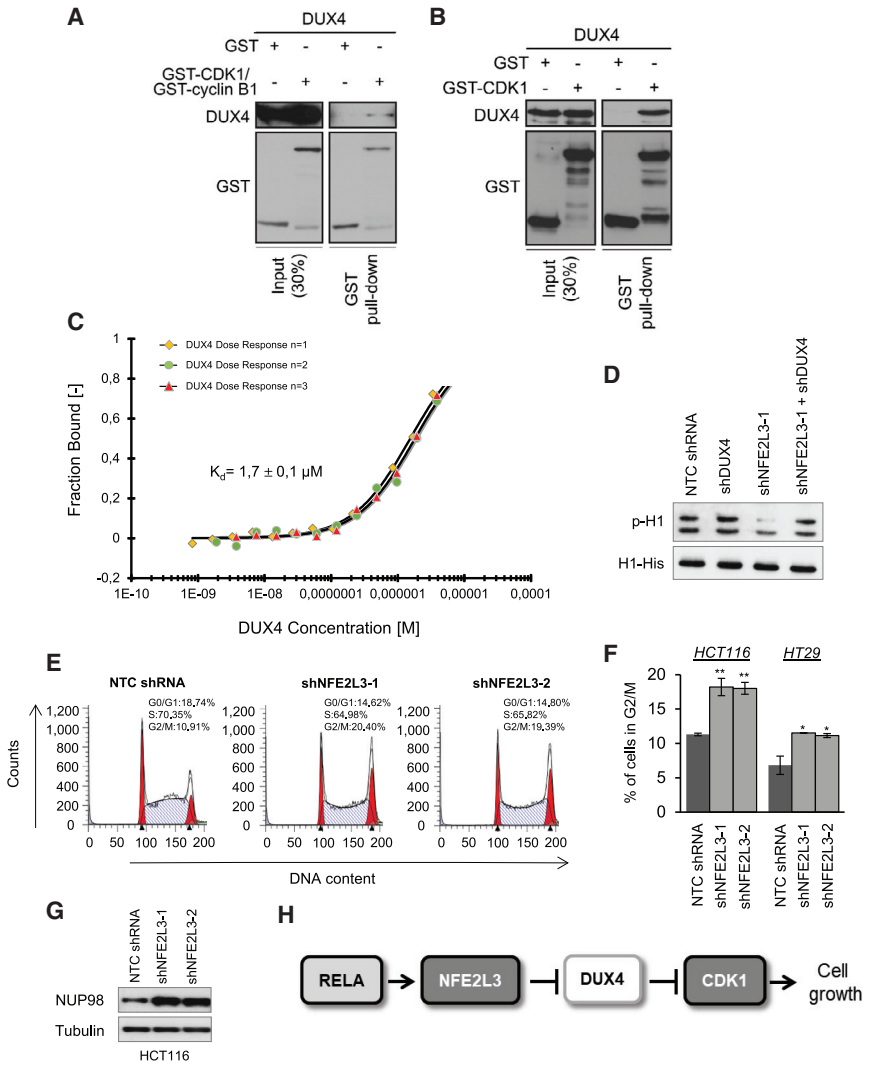

Figure 6. DUX4 Interacts Directly with CDK1 and Inhibits Its Activity

(A) *In vitro* GST pull-down of recombinant GST or GST-CDK1/GST-cyclin B1 and recombinant DUX4-Myc-FLAG using glutathione beads.

(B) *In vitro* GST pull-down of recombinant GST or GST-CDK1 and recombinant DUX4-Myc-FLAG using glutathione beads. Lysate and pull-down were immunoblotted for the indicated proteins (signals shown for each antibody are from the same exposition time).

(C) Microscale thermophoresis analysis for dissociation constant determination between GST-DUX4 and human CDK1. K_D value is shown. The different-colored lines correspond to the different replicates of the MST dose-response curves (n = 3). GST alone was used as a negative control.

(D) Immunoblots of indicated proteins after *in vitro* kinase assay containing ATP, His-H1, and immunoprecipitated CDK1 complexes from HCT116 cells transduced with a NTC shRNA, a NFE2L3-specific shRNA (shNFE2L3-1), a DUX4-specific shRNA (shDUX4), or both (shNFE2L3-1, shDUX4).

(E) Cell-cycle distribution of HCT116 cells transduced with a NTC shRNA or NFE2L3-specific shRNAs (shNFE2L3-1 or -2) assessed by flow cytometry after PI staining.

(F) Percentage of HCT116 and HT29 cells treated as in (E) in the G2/M phase. Error bars are means ± SEM, n = 3 independent experiments, *p < 0.05, **p < 0.01, two-sided Student's t test.

(G) Immunoblot analysis of NUP98 and tubulin in HCT116 cells as in (E).

(H) Model for the pathway of the RELA and NFE2L3 transcription factors controlling cell-cycle progression via the regulation of DUX4 and CDK1.

we found that the region between aa 111 and 180 mediates the DUX4-CDK1 interaction. Our *in silico* analysis predicted that the DUX4 residues Arg117 and Phe118 are among the key amino acids mediating that interaction (Figure S6). We generated point mutants of DUX4 in these two residues and indeed observed a reduced interaction between these two mutants and CDK1 in coIP studies (Figure 5G). The molecular mechanisms controlling cell-cycle progression are complex, requiring the coordinated action of a series of regulatory proteins, including major tumor suppressors, such as the cyclin-dependent kinase inhibitor 1A (CDKN1A; p21), cyclin-dependent kinase inhibitor 2A (CDKN2A; p16), and retinoblastoma (RB) proteins (Asghar et al., 2015; Liggett and Sidransky, 1998). Deficient control of the cell cycle may lead to transformation of normal cells and enhance tumor development. CDK1-cyclin B1, a serine/threonine kinase complex regulated through protein-protein interactions and post-transcriptional modifications, has a major role in G2/M phase transition (Santamaría et al., 2007). With respect to the mechanism explaining the effect of NFE2L3 on cell-cycle progression, we hypothesize that DUX4 binds directly to CDK1 and limits the interaction with its targets that are phosphorylated by the enzyme (Brown et al., 2015). As the overexpression of exogenous wild-type DUX4, driven by a regular, and even by a weak, promoter, is highly toxic to the cells, we could not use wild-type DUX4, and in parallel the non-CDK binding mutants, to determine their effect on the activity of CDK1. In addition, our GST pull-down data suggest that DUX4 preferentially interacts with CDK1 alone. However, an assay to assess the inhibition of kinase activity with only recombinant CDK1, which is inactive without cyclin B1, is not feasible. However, we have shown in our *in vitro* kinase assay that inhibition of CDK1 is dependent upon direct binding of DUX4 because the combined NFE2L3/DUX4 knockdown does not lead to a decrease in H1 phosphorylation in contrast to NFE2L3 knockdown alone (Figure 6D). Nevertheless, complementary experiments are required to determine whether DUX4 is a specific inhibitor of CDK1 or also can inhibit the activity of other CDKs, for example, CDK2, CDK4, or CDK6. Because of their central role in cell-cycle progression, CDKs have been a major target for cancer therapy (Asghar et al., 2015). For example, the CDK4/6 inhibitor palbociclib has been approved recently for use in patients with breast cancer (Finn et al., 2016). Current challenges are in the

development of highly selective agents against specific CDKs, companion diagnostics that will enable the selection of appropriate patient populations, and a better understanding of the intersection of pharmacology and biology that will provide the basis for rational drug combinations (Asghar et al., 2015). Our finding that DUX4, which is tightly regulated by NFE2L3, functions as a direct inhibitor of CDK1, will open novel treatment opportunities by precision therapy, for example, by screening for molecules that inhibit NFE2L3 activity or promote DUX4 expression in tumors.

Taken together, based on our observations, we propose the existence of an oncogenic pathway, comprising the RELA, NFE2L3, DUX4, and CDK1 proteins that control colon cancer cell growth. Our study establishes a key role for the NFE2L3 transcription factor that regulates cell-cycle progression by governing the expression of DUX4, a direct inhibitor of CDK1.

STAR★METHODS

Detailed methods are provided in the online version of this paper and include the following:

- KEY RESOURCES TABLE
- LEAD CONTACT AND MATERIALS AVAILABILITY
- EXPERIMENTAL MODEL AND SUBJECT DETAILS
  - Tissue Microarray and Patient Samples
  - Mouse Xenograft Study
  - Cell Lines
- METHOD DETAILS
  - Reagents
  - Lentivirus-Based Transduction of Cells with shRNA
  - RNA Extraction and RT-qPCR
  - Immunoblot
  - Cell Proliferation and Survival Assay
  - Clonogenic and Soft Agar Assays
  - Apoptosis and Cell Cycle Analysis
  - Immunohistochemistry
  - ChIP-qPCR and ChIP-Seq
  - Dual-luciferase Reporter Assay
  - (Co-)Immunoprecipitation
  - Mass Spectrometry
  - Prediction of DUX4 Structure using Fold Recognition Domain
  - Modeling DUX4-CDK1 Complex
  - *In Vitro* Protein Interaction (GST Pull-down Assay)
  - Purification of GST-DUX4
  - Microscale Thermophoresis (MST)
  - Kinase Assay
- QUANTIFICATION AND STATISTICAL ANALYSIS
  - Statistical Methods
- DATA AND CODE AVAILABILITY
  - ChIP-seq Data Link
  - TMA Link

SUPPLEMENTAL INFORMATION

Supplemental Information can be found online at https://doi.org/10.1016/j.celrep.2019.09.087.

ACKNOWLEDGMENTS

We would like to thank Joo Yeoun Park, Isadore Dodard-Freedman, Meenakshi Kannan, Yusra Kassim, Stéphane Richard, Koren Mann, Eric Milot, Colin Crist, Johan Wouters, Guido Bommer, and Alain Israël for reading of the manuscript and/or valuable discussions and/or material support. We would like to thank Alan Spatz and Leon van Kempen (JGH, Montreal) for human colon cancer samples and Jose Torres for analysis of pathology specimens. We would like to acknowledge the LDI Flow Cytometry Facility (LDI, Montreal) for their flow cytometry technical expertise and the ENCODE project consortium and the ENCODE production laboratory for generating the dataset. Bioinformatics analyses were performed at the Bioinformatics Core Facility at the Institute for Research in Immunology and Cancer (IRIC), Université de Montréal (Montreal, QC, Canada). Proteomics analyses were performed by the Center for Advanced Proteomics Analyses (IRIC), a Node of the Canadian Genomic Innovation Network that is supported by the Canadian Government through Genome Canada. We also would like to thank Léopold Thabault and Raphaël Frédérick for access to the microscale thermophoresis platform (UCLouvain, Brussels) and Jocelyn Eidahl (Nationwide Children's Hospital, USA) and Frédérique Coppée (UMons, Mons) for the DUX4-GST plasmid. M.B. was supported by fellowships from McGill Integrated Cancer Research Training Program (MICRTP, Canada), Le Fonds de recherche du Québec - Santé (FRQS, Canada), and the Cole Foundation (Canada); B.L.C. was supported by Télévie fellowship (FNRS, Belgium); F.L. was supported by FRQS and CRS (Cancer Research Society, Canada) postdoctoral fellowships; T.D.M was supported by Fund for Research training in Industry and Agriculture (FRIA, Belgium); and J.S. was supported by SEG (Lebanon) and MICRTP studentships. The research was supported by grants from the Canadian Institutes of Health Research (CIHR, Canada) MOP-97932 and PJT-152937 to V.B.

AUTHOR CONTRIBUTIONS

Conceptualization, M.B., B.L.C., and V.B.; Methodology, M.B. and B.L.C.; Investigation and Validation, M.B., B.L.C., F.L., T.D.M., and J.S.; Resources, C.M., G.F., and V.B.; Writing – Original Draft, M.B., B.L.C., and V.B.; Writing – Review & Editing, M.B., B.L.C., and V.B.; Visualization, M.B.; Supervision, C.M., G.F., and V.B.; Funding Acquisition, V.B.

DECLARATION OF INTERESTS

The authors declare no competing interests.

Received: July 12, 2018
Revised: June 26, 2019
Accepted: September 27, 2019
Published: November 5, 2019

SUPPORTING CITATIONS

The following citations appear in the Supplemental Information: McCall et al. (2011); Rhodes et al. (2004); Wu et al. (2009).

REFERENCES

Aggarwal, B.B., and Sung, B. (2011). NF-κB in cancer: a matter of life and death. Cancer Discov. *1*, 469–471.

Al Obeed, O.A., Alkhayal, K.A., Al Sheikh, A., Zubaidi, A.M., Vaali-Mohammed, M.A., Boushey, R., Mckerrow, J.H., and Abdulla, M.H. (2014). Increased expression of tumor necrosis factor-α is associated with advanced colorectal cancer stages. World J. Gastroenterol. *20*, 18390–18396.

Asghar, U., Witkiewicz, A.K., Turner, N.C., and Knudsen, E.S. (2015). The history and future of targeting cyclin-dependent kinases in cancer therapy. Nat. Rev. Drug Discov. *14*, 130–146.

Ben-Neriah, Y., and Karin, M. (2011). Inflammation meets cancer, with NF-κB as the matchmaker. Nat. Immunol. *12*, 715–723.

Bosnakovski, D., Xu, Z., Gang, E.J., Galindo, C.L., Liu, M., Simsek, T., Garner, H.R., Agha-Mohammadi, S., Tassin, A., Coppée, F., et al. (2008). An isogenetic myoblast expression screen identifies DUX4-mediated FSHD-associated molecular pathologies. EMBO J. *27*, 2766–2779.

Brenner, H., Kloor, M., and Pox, C.P. (2014). Colorectal cancer. Lancet *383*, 1490–1502.

Brown, N.R., Korolchuk, S., Martin, M.P., Stanley, W.A., Moukhametzianov, R., Noble, M.E.M., and Endicott, J.A. (2015). CDK1 structures reveal conserved and unique features of the essential cell cycle CDK. Nat. Commun. *6*, 6769.

Cancer Genome Atlas Network (2012). Comprehensive molecular characterization of human colon and rectal cancer. Nature *487*, 330–337.

Chénais, B., Derjuga, A., Massrieh, W., Red-Horse, K., Bellingard, V., Fisher, S.J., and Blank, V. (2005). Functional and placental expression analysis of the human NRF3 transcription factor. Mol. Endocrinol. *19*, 125–137.

Chevillard, G., and Blank, V. (2011). NFE2L3 (NRF3): the Cinderella of the Cap'n'Collar transcription factors. Cell. Mol. Life Sci. *68*, 3337–3348.

Chevillard, G., Paquet, M., and Blank, V. (2011). Nfe2l3 (Nrf3) deficiency predisposes mice to T-cell lymphoblastic lymphoma. Blood *117*, 2005–2008.

Chowdhury, A.M.M.A., Katoh, H., Hatanaka, A., Iwanari, H., Nakamura, N., Hamakubo, T., Natsume, T., Waku, T., and Kobayashi, A. (2017). Multiple regulatory mechanisms of the biological function of NRF3 (NFE2L3) control cancer cell proliferation. Sci. Rep. *7*, 12494.

Chu, D., Zhou, Y., Zhang, Z., Li, Y., Li, J., Zheng, J., Zhang, H., Zhao, Q., Wang, W., Wang, R., and Ji, G. (2011). Notch1 expression, which is related to p65 Status, is an independent predictor of prognosis in colorectal cancer. Clin. Cancer Res. *17*, 5686–5694.

Coxon, C.R., Anscombe, E., Harnor, S.J., Martin, M.P., Carbain, B., Golding, B.T., Hardcastle, I.R., Harlow, L.K., Korolchuk, S., Matheson, C.J., et al. (2017). Cyclin-Dependent Kinase (CDK) Inhibitors: Structure-Activity Relationships and Insights into the CDK-2 Selectivity of 6-Substituted 2-Arylaminopurines. J. Med. Chem. *60*, 1746–1767.

Dan, H.C., Cooper, M.J., Cogswell, P.C., Duncan, J.A., Ting, J.P., and Baldwin, A.S. (2008). Akt-dependent regulation of NF-kappaB is controlled by mTOR and Raptor in association with IKK. Genes Dev. *22*, 1490–1500.

De Sousa E Melo, F., Wang, X., Jansen, M., Fessler, E., Trinh, A., de Rooij, L.P., de Jong, J.H., de Boer, O.J., van Leersum, R., Bijlsma, M.F., et al. (2013). Poor-prognosis colon cancer is defined by a molecularly distinct subtype and develops from serrated precursor lesions. Nat. Med. *19*, 614–618.

DeNicola, G.M., Karreth, F.A., Humpton, T.J., Gopinathan, A., Wei, C., Frese, K., Mangal, D., Yu, K.H., Yeo, C.J., Calhoun, E.S., et al. (2011). Oncogene-induced Nrf2 transcription promotes ROS detoxification and tumorigenesis. Nature *475*, 106–109.

Dmitriev, P., Kiseleva, E., Kharchenko, O., Ivashkin, E., Pichugin, A., Dessen, P., Robert, T., Coppée, F., Belayew, A., Carnac, G., et al. (2016). Dux4 controls migration of mesenchymal stem cells through the Cxcr4-Sdf1 axis. Oncotarget *7*, 65090–65108.

Eidahl, J.O., Giesige, C.R., Domire, J.S., Wallace, L.M., Fowler, A.M., Guckes, S., Garwick-Coppens, S., Labhart, P., and Harper, S.Q. (2016). Mouse Dux is myotoxic and shares partial functional homology with its human paralog DUX4. Hum. Mol. Genet. *25*, 4577–4589.

ENCODE Project Consortium (2012). An integrated encyclopedia of DNA elements in the human genome. Nature *489*, 57–74.

Finn, R.S., Crown, J.P., Ettl, J., Schmidt, M., Bondarenko, I.M., Lang, I., Pinter, T., Boer, K., Patel, R., Randolph, S., et al. (2016). Efficacy and safety of palbociclib in combination with letrozole as first-line treatment of ER-positive, HER2-negative, advanced breast cancer: expanded analyses of subgroups from the randomized pivotal trial PALOMA-1/TRIO-18. Breast Cancer Res. *18*, 67.

Gabellini, D., Green, M.R., and Tupler, R. (2002). Inappropriate gene activation in FSHD: a repressor complex binds a chromosomal repeat deleted in dystrophic muscle. Cell *110*, 339–348.

Heinz, S., Benner, C., Spann, N., Bertolino, E., Lin, Y.C., Laslo, P., Cheng, J.X., Murre, C., Singh, H., and Glass, C.K. (2010). Simple combinations of lineage-determining transcription factors prime cis-regulatory elements required for macrophage and B cell identities. Mol. Cell *38*, 576–589.

Hinz, M., Krappmann, D., Eichten, A., Heder, A., Scheidereit, C., and Strauss, M. (1999). NF-kappaB function in growth control: regulation of cyclin D1 expression and G0/G1-to-S-phase transition. Mol. Cell. Biol. *19*, 2690–2698.

Kannan, M.B., Dodard-Friedman, I., and Blank, V. (2015). Stringent Control of NFE2L3 (Nuclear Factor, Erythroid 2-Like 3; NRF3) Protein Degradation by FBW7 (F-box/WD Repeat-containing Protein 7) and Glycogen Synthase Kinase 3 (GSK3). J. Biol. Chem. *290*, 26292–26302.

Karin, M. (2006). Nuclear factor-kappaB in cancer development and progression. Nature *441*, 431–436.

Karin, M., Cao, Y., Greten, F.R., and Li, Z.W. (2002). NF-kappaB in cancer: from innocent bystander to major culprit. Nat. Rev. Cancer *2*, 301–310.

Kawamura-Saito, M., Yamazaki, Y., Kaneko, K., Kawaguchi, N., Kanda, H., Mukai, H., Gotoh, T., Motoi, T., Fukayama, M., Aburatani, H., et al. (2006). Fusion between CIC and DUX4 up-regulates PEA3 family genes in Ewing-like sarcomas with t(4;19)(q35;q13) translocation. Hum. Mol. Genet. *15*, 2125–2137.

Kuipers, E.J., Grady, W.M., Lieberman, D., Seufferlein, T., Sung, J.J., Boelens, P.G., van de Velde, C.J., and Watanabe, T. (2015). Colorectal cancer. Nat. Rev. Dis. Primers *1*, 15065.

La Rosa, F.A., Pierce, J.W., and Sonenshein, G.E. (1994). Differential regulation of the c-myc oncogene promoter by the NF-kappa B rel family of transcription factors. Mol. Cell. Biol. *14*, 1039–1044.

Laurell, E., Beck, K., Krupina, K., Theerthagiri, G., Bodenmiller, B., Horvath, P., Aebersold, R., Antonin, W., and Kutay, U. (2011). Phosphorylation of Nup98 by multiple kinases is crucial for NPC disassembly during mitotic entry. Cell *144*, 539–550.

Lessard, F., Igelmann, S., Trahan, C., Huot, G., Saint-Germain, E., Mignacca, L., Del Toro, N., Lopes-Paciencia, S., Le Calvé, B., Montero, M., et al. (2018). Senescence-associated ribosome biogenesis defects contributes to cell cycle arrest through the Rb pathway. Nat. Cell Biol. *20*, 789–799.

Li, H., Handsaker, B., Wysoker, A., Fennell, T., Ruan, J., Homer, N., Marth, G., Abecasis, G., and Durbin, R.; 1000 Genome Project Data Processing Subgroup (2009). The Sequence Alignment/Map format and SAMtools. Bioinformatics *25*, 2078–2079.

Li, S., Pinard, M., Wang, Y., Yang, L., Lin, R., Hiscott, J., Su, B., and Brodt, P. (2015). Crosstalk between the TNF and IGF pathways enhances NF-κB activation and signaling in cancer cells. Growth Horm. IGF Res. *25*, 253–261.

Liggett, W.H., Jr., and Sidransky, D. (1998). Role of the p16 tumor suppressor gene in cancer. J. Clin. Oncol. *16*, 1197–1206.

McCall, M.N., Uppal, K., Jaffee, H.A., Zilliox, M.J., and Irizarry, R.A. (2011). The Gene Expression Barcode: leveraging public data repositories to begin cataloging the human and murine transcriptomes. Nucleic Acids Res. *39*, D1011–D1015.

Mintseris, J., Pierce, B., Wiehe, K., Anderson, R., Chen, R., and Weng, Z. (2007). Integrating statistical pair potentials into protein complex prediction. Proteins *69*, 511–520.

Nouhi, Z., Chevillard, G., Derjuga, A., and Blank, V. (2007). Endoplasmic reticulum association and N-linked glycosylation of the human Nrf3 transcription factor. FEBS Lett. *581*, 5401–5406.

Perkins, N.D., Felzien, L.K., Betts, J.C., Leung, K., Beach, D.H., and Nabel, G.J. (1997). Regulation of NF-kappaB by cyclin-dependent kinases associated with the p300 coactivator. Science *275*, 523–527.

Pierce, J.W., Schoenleber, R., Jesmok, G., Best, J., Moore, S.A., Collins, T., and Gerritsen, M.E. (1997). Novel inhibitors of cytokine-induced IkappaBalpha phosphorylation and endothelial cell adhesion molecule expression show anti-inflammatory effects in vivo. J. Biol. Chem. *272*, 21096–21103.

Pierce, B.G., Hourai, Y., and Weng, Z. (2011). Accelerating protein docking in ZDOCK using an advanced 3D convolution library. PLoS ONE *6*, e24657.

Rezapour, S., Bahrami, T., Hashemzadeh, S., Estiar, M.A., Nemati, M., Ravanbakhsh, R., Feizi, M.A., Kafil, H.S., Pouladi, N., Ghojazadeh, M., and Sakhinia, E. (2016). STC1 and NF-κB p65 (Rel A) is Constitutively Activated in Colorectal Cancer. Clin. Lab. *62*, 463–469.

Rhodes, D.R., Yu, J., Shanker, K., Deshpande, N., Varambally, R., Ghosh, D., Barrette, T., Pandey, A., and Chinnaiyan, A.M. (2004). ONCOMINE: a cancer microarray database and integrated data-mining platform. Neoplasia *6*, 1–6.

Roy, A., Kucukural, A., and Zhang, Y. (2010). I-TASSER: a unified platform for automated protein structure and function prediction. Nat. Protoc. *5*, 725–738.

Ruiz, E.J., Vilar, M., and Nebreda, A.R. (2010). A two-step inactivation mechanism of Myt1 ensures CDK1/cyclin B activation and meiosis I entry. Curr. Biol. *20*, 717–723.

Santamaría, D., Barrière, C., Cerqueira, A., Hunt, S., Tardy, C., Newton, K., Cáceres, J.F., Dubus, P., Malumbres, M., and Barbacid, M. (2007). Cdk1 is sufficient to drive the mammalian cell cycle. Nature *448*, 811–815.

Schwitalla, S., Fingerle, A.A., Cammareri, P., Nebelsiek, T., Göktuna, S.I., Ziegler, P.K., Canli, O., Heijmans, J., Huels, D.J., Moreaux, G., et al. (2013). Intestinal tumorigenesis initiated by dedifferentiation and acquisition of stem-cell-like properties. Cell *152*, 25–38.

Shin, H.M., Kim, M.H., Kim, B.H., Jung, S.H., Kim, Y.S., Park, H.J., Hong, J.T., Min, K.R., and Kim, Y. (2004). Inhibitory action of novel aromatic diamine compound on lipopolysaccharide-induced nuclear translocation of NF-kappaB without affecting IkappaB degradation. FEBS Lett. *571*, 50–54.

Siegenthaler, B., Defila, C., Muzumdar, S., Beer, H.D., Meyer, M., Tanner, S., Bloch, W., Blank, V., Schäfer, M., and Werner, S. (2018). Nrf3 promotes UV-induced keratinocyte apoptosis through suppression of cell adhesion. Cell Death Differ. *25*, 1749–1765.

Singh, C. (2017). Staging of Colonic Carcinoma, 7th edition (AJCC). http://www.pathologyoutlines.com/topic/colontumorstaging.html.

Sun, J., Zheng, Z., Chen, Q., Pan, Y., Lu, H., Zhang, H., Yu, Y., and Dai, Y. (2019). NRF3 suppresses breast cancer cell metastasis and cell proliferation and is a favorable predictor of survival in breast cancer. OncoTargets Ther. *12*, 3019–3030.

Szlosarek, P., Charles, K.A., and Balkwill, F.R. (2006). Tumour necrosis factor-alpha as a tumour promoter. Eur. J. Cancer *42*, 745–750.

The UniProt Consortium (2017). UniProt: the universal protein knowledgebase. Nucleic Acids Res. *45* (*D1*), D158–D169.

Vaiopoulos, A.G., Papachroni, K.K., and Papavassiliou, A.G. (2010). Colon carcinogenesis: Learning from NF-kappaB and AP-1. Int. J. Biochem. Cell Biol. *42*, 1061–1065.

Vaiopoulos, A.G., Athanasoula, K.Ch., and Papavassiliou, A.G. (2013). NF-κB in colorectal cancer. J. Mol. Med. (Berl.) *91*, 1029–1037.

van den Heuvel, S., and Harlow, E. (1993). Distinct roles for cyclin-dependent kinases in cell cycle control. Science *262*, 2050–2054.

Vinson, K.E., George, D.C., Fender, A.W., Bertrand, F.E., and Sigounas, G. (2016). The Notch pathway in colorectal cancer. Int. J. Cancer *138*, 1835–1842.

Wang, S., Liu, Z., Wang, L., and Zhang, X. (2009). NF-kappaB signaling pathway, inflammation and colorectal cancer. Cell. Mol. Immunol. *6*, 327–334.

Wang, C., Saji, M., Justiniano, S.E., Yusof, A.M., Zhang, X., Yu, L., Fernández, S., Wakely, P., Jr., La Perle, K., Nakanishi, H., et al. (2017). RCAN1-4 is a thyroid cancer growth and metastasis suppressor. JCI Insight *2*, e90651.

Wang, H., Zhan, M., Yang, R., Shi, Y., Liu, Q., and Wang, J. (2018). Elevated expression of NFE2L3 predicts the poor prognosis of pancreatic cancer patients. Cell Cycle *17*, 2164–2174.

Wu, S., and Zhang, Y. (2007). LOMETS: a local meta-threading-server for protein structure prediction. Nucleic Acids Res. *35*, 3375–3382.

Wu, C., Orozco, C., Boyer, J., Leglise, M., Goodale, J., Batalov, S., Hodge, C.L., Haase, J., Janes, J., Huss, J.W., 3rd, and Su, A.I. (2009). BioGPS: an extensible and customizable portal for querying and organizing gene annotation resources. Genome Biol. *10*, R130.

Wu, D., Wu, P., Zhao, L., Huang, L., Zhang, Z., Zhao, S., and Huang, J. (2015). NF-κB Expression and Outcomes in Solid Tumors: A Systematic Review and Meta-Analysis. Medicine (Baltimore) *94*, e1687.

Yang, J., Yan, R., Roy, A., Xu, D., Poisson, J., and Zhang, Y. (2015). The I-TASSER Suite: protein structure and function prediction. Nat. Methods *12*, 7–8.

Yasuda, T., Tsuzuki, S., Kawazu, M., Hayakawa, F., Kojima, S., Ueno, T., Imoto, N., Kohsaka, S., Kunita, A., Doi, K., et al. (2016). Recurrent DUX4 fusions in B cell acute lymphoblastic leukemia of adolescents and young adults. Nat. Genet. *48*, 569–574.

Yu, G., and He, Q.Y. (2016). ReactomePA: an R/Bioconductor package for reactome pathway analysis and visualization. Mol. Biosyst. *12*, 477–479.

Zhang, Y. (2008). I-TASSER server for protein 3D structure prediction. BMC Bioinformatics *9*, 40.

Zhang, J., McCastlain, K., Yoshihara, H., Xu, B., Chang, Y., Churchman, M.L., Wu, G., Li, Y., Wei, L., Iacobucci, I., et al.; St. Jude Children's Research Hospital–Washington University Pediatric Cancer Genome Project (2016). Deregulation of DUX4 and ERG in acute lymphoblastic leukemia. Nat. Genet. *48*, 1481–1489.

Zhang, Q., Lenardo, M.J., and Baltimore, D. (2017). 30 Years of NF-κB: a blossoming of relevance to human pathobiology. Cell *168*, 37–57.

STAR★METHODS

KEY RESOURCES TABLE

REAGENT or RESOURCE	SOURCE	IDENTIFIER
Antibodies		
Rabbit anti-NFE2L3	Kannan et al., 2015	N/A
Biotin-SP-conjugated Affinipure Donkey anti-rabbit IgG	Jackson Immuno Research	Cat# 711-065-152
Rabbit polyclonal anti Pol-II (N-20)	Santa Cruz	Cat# sc-899 RRID:AB_632359
		Lot# G3014
Rabbit polyclonal anti-RELA (A)	Santa Cruz	Cat# sc-109X RRID:AB_632039
		Lot# L0814
Rabbit polyclonal anti-NFKB1 (H-119)	Santa Cruz	Cat# sc-7178 RRID:AB_650211
Rabbit polyclonal anti-REL (N)	Santa Cruz	Cat# sc-70 RRID:AB_2178727
		Lot# B1814
Rabbit polyclonal anti-RELB (C-19)	Santa Cruz	Cat# sc-226 RRID:AB_X632341
Mouse monoclonal anti-DUX4 (C-2)	Santa Cruz	Cat# sc-376490 RRID:AB_11151782
		Lot# D1514
Mouse monoclonal anti-CDK1 (17)	Santa Cruz	Cat# sc-54 RRID:AB_627224
		Lot# K1915
Rabbit monoclonal anti-CDK1 (PSTAIRE)	Santa Cruz	Cat# sc-53 RRID:AB_2074908
		Lot# F2714
Mouse monoclonal anti-HA-Tag (F-7)	Santa Cruz	Cat# sc-7392 RRID:AB_627809
		Lot# E1718
Normal rabbit IgG	Santa Cruz	Cat# sc-2027 RRID:AB_737197
		Lot# H2615
Normal mouse IgG	Santa Cruz	Cat# sc-2025 RRID:AB_737182
		Lot# H0615
Rabbit polyclonal anti-NFKB2	Cell Signaling	Cat# 4882S RRID:AB_10695537
		Lot# 4
Rabbit monoclonal anti-phospho-RELA (93H1)	Cell Signaling	Cat# 3033S RRID:AB_331284
		Lot# 14
Rabbit monoclonal anti-phospho-NFKBIA (14D4)	Cell Signaling	Cat# 2859S RRID:AB_561111
		Lot#14
Rabbit monoclonal anti-Myc-Tag (9B11)	Cell Signaling	Cat# 2276 RRID:AB_331783
		Lot# 24
Rabbit monoclonal anti-NUP98 (C39A3)	Cell Signaling	Cat# 2598 RRID:AB_2267700
		Lot# 4
Mouse monoclonal anti-α-Tubulin (B-5-1-2)	Sigma-Aldrich	Cat# T6074 RRID:AB_477582
		Lot# 075M4823V
Mouse monoclonal anti-His-Tag	QIAGEN	Cat# 34660 RRID:AB_2619735
		Lot# 4
Mouse monoclonal anti-phospho-Histone H1 (12D11)	Merck Millipore	Cat# 05-1324 RRID:AB_1587115
		Lot# 3072319
Rabbit monoclonal anti-MKI67	BioCare Medical	Cat# CRM 325 A
Bacterial and Virus Strains		
E.coli BL21 (DE3)	NEB	C2527I

(*Continued on next page*)

Continued

REAGENT or RESOURCE	SOURCE	IDENTIFIER
Biological Samples		
Colon adenocarcinoma, 75 cases, Tumor and Matched NAT (tissue microarray)	Amsbio	Col150CS-01
Matched normal colon tissue and colorectal adenocarcinoma tissue samples (FFPE)	Jewish General Hospital Central Biobank (Montreal)	IRB approval number 15-149
Chemicals, Peptides, and Recombinant Proteins		
Tumor necrosis factor recombinant human protein	Invitrogen	Cat# PHC3011
BAY 11-7082 inhibitor	Santa Cruz	Cat# sc-200615; CAS 19542-67-7
JSH-23 inhibitor	Cedarlane	Cat# S7351; CAS 749886-87-1
LY294002 inhibitor	NEB	Cat# 9901
PD98059 inhibitor	NEB	Cat# 9900
SB-202190	Calbiochem	Cat# 559388; CAS 152121-30-7
Recombinant human DUX4-Myc-FLAG protein	This paper	N/A
Recombinant GST protein	Sigma-Aldrich	Cat# SRP5348
Recombinant human CDK1/CyclinB1	Sigma-Aldrich	Cat# SRP5009
Recombinant full-length human CDK1 protein	SignalChem	Cat# C22-14G
Recombinant human CDK1 protein	Abcam	Cat# ab187447
Recombinant human Histone H1 protein	Abcam	Cat# ab198676
FLAG Peptide	Sigma-Aldrich	Cat# F3290
Critical Commercial Assays		
Amplification kit	Roche	Cat# 760-080
DAB Map detection kit	Roche	Cat# 760-124
AllPrep DNA/RNA/Protein Mini kit	QIAGEN	Cat# 80004
Purelink HiPure Plasmid Maxiprep kit	Invitrogen	Cat# K210007
QuickChange II XL Site-Directed Mutagenesis kit	Agilent	Cat# 200522
EasyScript Plus cDNA Synthesis kit	Abmgood	Cat# G236
BrdU Cell Proliferation ELISA kit	Abcam	Cat# ab126556
Annexin V-FITC Apoptosis Detection kit	Sigma-Aldrich	Cat# APOAF
Bond Polymer DAB Refine kit	Leica Biosystems	Cat# DS9800
Dual-Luciferase Reporter Assay System	Promega	Cat# E1910
Deposited Data		
ChIP-seq data	This paper	https://onedrive.live.com/redir?resid=3F5A1FD25439B0CE!108&authkey=!APH0PPlEs_AqUw&ithint=folder%2c
TMA data	This paper	https://onedrive.live.com/redir?resid=3F5A1FD25439B0CE!109&authkey=!ACVMRj5FWUvVPZg
Mass spectrometry data	This paper	See Table S1
Experimental Models: Cell Lines		
Human colorectal carcinoma cells: HCT 116 cells	ATCC	CCL-247
Human colorectal adenocarcinoma cells: HT-29 cells	ATCC	HTB-38
Human embryonic kidney cells: HEK293T	ATCC	CRL-11268
Human embryonic kidney cells: HEK293	ATCC	CRL-1573
Experimental Models: Organisms/Strains		
Mice: Hsd: Athymic Nude-*Foxn1*^{nu}	Harlan Laboratories	N/A
Oligonucleotides		
Primers for NFE2L3, see Table S2	This paper	N/A
Primers for MKI67, see Table S2	This paper	N/A
Primers for DUX4, see Table S2	This paper	N/A

(*Continued on next page*)

Continued

REAGENT or RESOURCE	SOURCE	IDENTIFIER
Primers for RELA, see Table S2	This paper	N/A
Primers for RELB, see Table S2	This paper	N/A
Primers for REL, see Table S2	This paper	N/A
Primers for NFKB1, see Table S2	This paper	N/A
Primers for NFKB2, see Table S2	This paper	N/A
Primers for ACTINB, see Table S2	This paper	N/A
Primers for GAPDH, see Table S2	This paper	N/A
Primers for CDKN1A, see Table S2	This paper	N/A
Forward primer for NFE2L3-ChIP-qPCR: CCACAGTCATTCACAACGGA	This paper	N/A
Reverse primer for NFE2L3-ChIP-qPCR: GCAGCTGTTCCATACGTTTACA	This paper	N/A
Forward primer for DUX4-ChIP-qPCR: TCACCTTTGTCATCAGTTCAGG	This paper	N/A
Reverse primer forDUX4-ChIP-qPCR: TGATGTAACTCTTGTCTAAGCTCTGC	This paper	N/A
Non-target shRNA control	Sigma-Aldrich	SHC216
shRNA 1 targeting NFE2L3	Sigma-Aldrich	TRCN0000430385
shRNA 2 targeting NFE2L3	Sigma-Aldrich	TRCN0000013488
shRNA 1 targeting RELA	Sigma-Aldrich	TRCN0000014684
shRNA 2 targeting RELA	Sigma-Aldrich	TRCN0000014683
shRNA 1 targeting NFKB1	Sigma-Aldrich	TRCN0000006517
shRNA 2 targeting NFKB1	Sigma-Aldrich	TRCN0000006518
shRNA 1 targeting NFKB2	Sigma-Aldrich	TRCN0000356047
shRNA 2 targeting NFKB2	Sigma-Aldrich	TRCN0000355955
shRNA 1 targeting REL	Sigma-Aldrich	TRCN0000039984
shRNA 2 targeting REL	Sigma-Aldrich	TRCN0000039983
shRNA 1 targeting RELB	Sigma-Aldrich	TRCN0000014713
shRNA 2 targeting RELB	Sigma-Aldrich	TRCN0000014714
Recombinant DNA		
pCMV-VSV-G	R. Weinberg's laboratory	Addgene plasmid #8454
pCMV-dR8.91	D. Trono's laboratory	Addgene plasmid #12263
pLV-Hygro-CMV-hNFE2L3 Full form NM_004289.6)	VectorBuilder	N/A
pLV-Hygro-CMV-hNFE2L3 Forms A/B	This paper	N/A
pLV-Hygro-CMV-hNFE2L3 Form C	This paper	N/A
pLV-Hygro-CMV-empty	VectorBuilder	N/A
pLV[shDUX4]-Hygro-U6 (CGAGTGGCTTTGCCCTCCCGA)	VectorBuilder	N/A
pLV[scramble shRNA]-Hygro-U6 (CCTAAGGTTAAGTCGC CCTCG)	VectorBuilder	N/A
pCMV4-RELA	W. Greene's laboratory	Addgene plasmid #21966
pCMV6-entry-Myc-Flag	Origene	PS100001
pCMV6-DUX4-Myc-Flag	Origene	RC238145
pCMV-neo-CDK1-HA	S. Van den Heuvel's laboratory	Addgene plasmid #1888
pCMV-neo-CDK2-HA	S. Van den Heuvel's laboratory	Addgene plasmid #1884
pCMV-neo-CDK4-HA	S. Van den Heuvel's laboratory	Addgene plasmid #1876
pCMV-neo-CDK6-HA	S. Van den Heuvel's laboratory	Addgene plasmid #1868
pCMV-HA-C	Clontech	635690
pcDNA3.1-Myc	Genscript	N/A
pcDNA3.1-DUX4(WT)-Myc	Genscript	N/A

(*Continued on next page*)

Continued

REAGENT or RESOURCE	SOURCE	IDENTIFIER
pcDNA3.1-DUX4(Δ111-131)-Myc	Genscript	N/A
pcDNA3.1-DUX4(Δ141-180)-Myc	Genscript	N/A
pcDNA3.1-DUX4(Δ381-400)-Myc	Genscript	N/A
pcDNA3.1-DUX4(Arg117Ala)-Myc	Genscript	N/A
pcDNA3.1-DUX4(Phe118Ala)-Myc	Genscript	N/A
GST-tagged DUX4 (pGEX-6-p1)	S. Harper's laboratory	N/A
Software and Algorithms		
SAMtools	Li et al., 2009	http://www.htslib.org
HOMER	Heinz et al., 2010	http://homer.ucsd.edu/homer/
PEAKS 7.0	Bio-informatics Solutions	N/A
I-TASSER	Roy et al., 2010; Yang et al., 2015; Zhang,2008	https://zhanglab.ccmb.med.umich.edu/I-TASSER/
LOMETS	Wu and Zhang, 2007	https://zhanglab.ccmb.med.umich.edu/LOMETS/
ZDOCK 3.0.2	Mintseris et al., 2007; Pierce et al., 2011	http://zdock.umassmed.edu
Statistica software	StatSoft	N/A

LEAD CONTACT AND MATERIALS AVAILABILITY

Further information and requests for resources and reagents should be directed to and will be fulfilled by the Lead Contact, Volker Blank (volker.blank@mcgill.ca). Plasmids generated in this study are available from the Lead Contact without restriction.

EXPERIMENTAL MODEL AND SUBJECT DETAILS

Tissue Microarray and Patient Samples

Colon cancer tissue microarray (Col150CS-01) was purchased from Amsbio, including 75 colon adenocarcinoma samples with matched normal adjacent tissues samples. Sections were deparaffinized inside an immunostainer. Antigen recovery was conducted using heat retrieval (Heat-Induced Epitope Retrieval) with CC1 (Ventana Medical Systems proprietary cell conditioner using a high pH buffer) for about 1 hour. Sections were then incubated with 100 μL of anti-NFE2L3 antiserum (see below) for 8 hours at room temperature. An amplification kit (760-080, Ventana Medical Systems - Roche) including rabbit anti-mouse IgG heavy and light chains and mouse anti-rabbit IgG heavy chains to bind to the primary antibody was applied to increase the staining intensity. Specific signal was acquired using DABmap detection kit (760-124, Ventana Medical Systems - Roche) according to provider's recommendations and a Biotin-SP-conjugated Affinipure Donkey Anti-Rabbit IgG (Jackson Immuno Research, 1/100) for 1 hour at room temperature. Slides were counterstained manually with Hematoxylin. Stained slides were coverslipped and scanned using the Hamamatsu's NanoZoomer® Digital Pathology system 2HT. We obtained five matched normal and colorectal tumor tissue samples from patients from the Jewish General Hospital Central Biobank (Montreal) with appropriate informed consent after approval by the Research Ethics Committee. The patients 298, 773 and 953 were male while the patients 315 and 626 were female. To determine the expression levels of *NFE2L3* mRNA, the AllPrep DNA/RNA/Protein Mini Kit (QIAGEN) was used following manufacturer's instructions.

Mouse Xenograft Study

Six- to seven-week-old female athymic *nu/nu* mice (Harlan) were inoculated with 2.5×10^6 HCT116 human colorectal cancer cells suspended in Matrigel: PBS (1:1; BD Biosciences) subcutaneously into their right flank. Tumor growth was monitored three times per week in three dimensions using a digital caliper. Tumor volumes were calculated with the modified ellipsoidal formula (LxWxH)/2, where L is length, W is width and H is height. Xenografts were harvested for subsequent analyses when they reached ~0.5 cm^3. Mice were housed under pathogen-free conditions, with food and water provided *ad libitum.* Procedures involving animals and their care were conducted according to McGill University guidelines, which are set by the Canadian Council on Animal Care.

Cell Lines

The HCT116 (from male) and HT29 (from female) human colon carcinoma cell lines used in this study were obtained from the American Type Culture Collection. These cells were cultured in RPMI 1640 media (Invitrogen) supplemented with 10% fetal bovine serum, 100 units/ml penicillin and 100 μg/ml streptomycin at 37°C with 5% CO_2.

METHOD DETAILS

Reagents

TNF was purchased from Invitrogen and the inhibitors of the NF-κB pathway, BAY 11-7082 and JSH-23 were bought from Santa Cruz and Cedarlane, respectively. LY294002 and PD98059 were purchased from NEB and SB-202190 from Calbiochem.

Lentivirus-Based Transduction of Cells with shRNA

Glycerol stocks of shRNA hairpins were obtained from the Sigma Mission library and isolation of plasmids was carried out with the PureLink® HiPure Plasmid Maxiprep Kit (Invitrogen). HEK293T cells were seeded 24 hours before transfection. For each 10-cm dish, 0.5 mL 2xHeBS (274 mM NaCl, 10 mM KCl, 1.5 mM $Na_2HPO_4.2H_2O$, 12 mM Dextrose, 50 mM HEPES in 500 mL MilliQ water at pH 7.01) was added into a sterile eppendorf tube. In another sterile eppendorf tube, 3 μg of plasmid DNA of interest, 2 μg of packaging vector pCMV-dR8.91, 1 μg of pCMV-VSV-G envelope vector, 60 μl of 2 M $CaCl_2$ and distilled water were added to bring up to 0.5 ml. The $CaCl_2$/plasmid DNA mix was added to the 2xHeBS and incubated for 20 min and then added to the cells. Medium was refreshed after 16 hours. The supernatant of HEK293T cells containing lentivirus was collected after 24 hours to infect cells with 5 μg/ml polybrene (Millipore) for 24 hours. The medium was refreshed after lentivirus infection and the cells were selected with puromycin and/or hygromycin. Individual shRNA vectors used were collected from the human TRC library (Sigma): TRC2 pLKO.5-puro Non-Target shRNA Control (NTC; SHC216); NFE2L3 sh1: TRCN0000430385; NFE2L3 sh2: TRCN0000013488; RELA sh1: TRCN0000014684; RELA sh2: TRCN0000014683; NFKB1 sh1: TRCN0000006517; NFKB1 sh2: TRCN0000006518; NFKB2 sh1: TRCN0000356047; NFKB2 sh2: TRCN0000355955; REL sh1: TRCN0000039984; REL sh2: TRCN0000039983; RELB sh1: TRCN0000014713; RELB sh2: TRCN0000014714. The pLV-Hygro-CMV-hNFE2L3[NM_004289.6], the corresponding empty vector, the pLV[shDUX4]-Hygro-U6 (CGAGTGGCTTTGCCCTCCCGA) and the pLV[scramble shRNA]-Hygro-U6 (CCTAAGGTTA AGTCGCCCTCG) were synthesized and cloned by VectorBuilder. We generated the AB and C mutants of NFE2L3 by mutating the pLV-Hygro-CMV-hNFE2L3 using Quikchange II XL (Agilent, 200522). The mutations targeting critical regions responsible for the generation of NFE2L3 A, B and C forms will be described in a different manuscript, Saliba et al., currently in preparation.

RNA Extraction and RT-qPCR

Total RNA was extracted using the TRizol-chloroform (Invitrogen) extraction method. Samples were digested with DNase I (Roche). cDNA was prepared using EasyScript Plus cDNA Synthesis Kit (Abmgood) according to the manufacturer's instructions. Transcript abundance was determined by qPCR using SsoAdvanced SYBR Green supermix (Bio-Rad) with primers in Table S2. qPCR analysis was performed in a CFX96 Touch Real Time PCR detection system (Bio-Rad). Data were analyzed by the threshold cycle (Ct) comparative method and normalized to ACTINB and GAPDH genes.

Immunoblot

Cells were lyzed with whole cell lysis buffer [10 mM Tris-HCl, pH 8.0, 420 mM NaCl, 250 mM sucrose, 2 mM $MgCl_2$, 1% Triton X-100, 1/100 cOmplete EDTA-free protease inhibitor cocktail (Roche), 1/25 PhosSTOP (Roche)] for 20 min on ice. Protein extracts were separated on CriterionTM XT (Bio-Rad) 4%–12% Bis-Tris gradient or Tris-glycine gels according to manufacturer's instructions. Proteins were then transferred to the PVDF membrane (Immobilon®-P, Millipore) in a wet transfer system in the absence of methanol. Membrane was blocked for 2-6 hours at room temperature in 5% milk in 1X TBS-T (50 mM Tris-HCl, pH 7.6, 200 mM NaCl, 0.05% Tween 20) and incubated with primary antibody overnight at 4°C. After 3 washes with 1X TBS-T, membrane was incubated for 1 hour with secondary antibody and washed at least 6 times with 1X TBS-T. The proteins were detected by Immobilon™ Western Chemiluminescent HRP substrate from Millipore according to instructions. We used an antiserum specific for a peptide (ENSLQQNDDDEN KIAEKPDWEAEK) of NFE2L3 (Kannan et al., 2015). The peptide was coupled to keyhole limpet hemocyanin and used to immunize female New Zealand White rabbits (Pocono Farms). The serum was purified using peptide coupled to Affi-Gel 10 (Biorad). Antibodies specific for the following proteins were purchased from Santa Cruz: Pol II (sc-899), RELA (sc-109), NFKB1 (sc-7178), REL (sc-70), RELB (sc-226), DUX4 (sc-376490), CDK1 (sc-53) and HA-tag (sc-7392). The antibodies specific for NFKB2 (4882), p-RELA (3033), p-NFKBIA (2859), Myc-Tag (2276) and NUP98 (2598) were purchased from Cell Signaling. The antibody specific for α-tubulin (T6074) was purchased from Sigma. The His-tag antibody (34660) was purchased from QIAGEN and the p-H1 (05-1324) antibody was purchased from Merck Millipore. Horseradish peroxidase (HRP)-conjugated secondary antibodies were purchased from Pierce and the VeriBlot Detection reagent (ab131365, Abcam) was used for immunoprecipitation.

Cell Proliferation and Survival Assay

BrdU incorporation assay was performed using the BrdU Cell Proliferation ELISA Kit (colorimetric) (Abcam). Briefly, HCT116 and HT29 cells were cultured in 96-well plates at a density of 1×10^3 cells/100 μl/well in complete growth media. After 60 hours, cells were labeled using 1x BrdU and incubated overnight at 37°C in a humidified atmosphere. After incubation, the culture medium was removed and cell DNA was denatured in one step by adding the fixing solution. Subsequently, the cells were incubated with the primary anti-BrdU monoclonal detector antibody for 1 hour at room temperature. Peroxidase Goat Anti Mouse IgG Conjugate was added after one washing step. After the removal of the antibody conjugate, the cells were washed and the TMB Peroxidase substrate was added for 30 min. The reaction product was quantified by measuring the absorbance using a microplate reader (Fluostar

Optima, BMG Labtech) at 450 nm. MTT assay was performed to detect cell viability after 72 hours by using Thiazolyl Blue Tetrazolium Bromide (MTT, Sigma) following the manufacturer's recommendations with an incubation of 4 hours at 37°C.

Clonogenic and Soft Agar Assays

For clonogenic assays, HCT116 and HT29 cells were plated at low density (1×10^3 cells per 6 cm dish) in fresh media. After 10 days, cells were stained with 0.5% (w/v) crystal violet in 25% methanol, and the number of colonies was counted. A soft agar assay was used to measure cell anchorage-independent growth. Cells were seeded into 6-well plates (coated with a basal layer made of 2 mL of 0.6% low-melting-point agarose) at 3×10^4 cells per well in 2 mL of 0.3% low-melting-point agarose containing 20% FBS). Two weeks after incubation, colonies were photographed and counted with an inverted microscope (Zeiss Primovert) equipped with a camera (Zeiss Axiocam ERc 5 s).

Apoptosis and Cell Cycle Analysis

The HCT116 and HT29 cell lines were trypsinized, centrifuged, aliquoted into tubes and labeled with annexin V and propidium iodide using an apoptosis detection kit (Sigma). Annexin V and PI staining were performed following the manufacturer's recommendations and analyzed with a BD FACSCalibur flow cytometer. For cell cycle analysis, subconfluent cells were synchronized by incubation in RPMI without FBS for 48 hours. Synchronized cells were then stimulated to proliferate by the addition of RPMI supplemented with 10% FBS. Cells were collected after 16 hours and fixed in 70% ethanol at −20°C overnight. The cells were washed with cold PBS, treated with 0.1 mg/ml of RNase A (Invitrogen), and stained with 50 μg/ml of propidium iodide (Sigma). Cell cycle profiles were analyzed by flow cytometry using the BD LSR Fortessa.

Immunohistochemistry

Immunohistochemical staining against NFE2L3 and MKI67 was carried out on paraffin-embedded formalin-fixed samples using the automated Bond RX staining platform from Leica Biosystems, Australia. Sections were deparaffinized inside an immunostainer. Antigen recovery was conducted using heat retrieval (Heat-Induced Epitope Retrieval) with ER2 (Leica Biosystems proprietary Epitope Retrieval using a high pH buffer) for 40 min. Sections were then incubated with 150 μL of anti-NFE2L3 antiserum (described above, 1/50) and 150 μL of anti-MKI67 antibody (Biocare Medical #CRM 325 A, 1/100) for 15 min at room temperature. Detection of specific signal was acquired by using Bond Polymer DAB Refine kit (#DS9800, Leica Biosystems) according to provider's recommendations. Slides were counterstained automatically with Hematoxylin included in the Polymer DAB kit. Stained slides were coverslipped and scanned using the Hamamatsu's NanoZoomer® Digital Pathology system 2HT.

ChIP-qPCR and ChIP-Seq

HCT116 cells were cross-linked using 1% formaldehyde for 10 min at room temperature and quenched with glycine to a final concentration of 0.125 M for 5 min. Subsequently, the cells were lysed in lysis buffer (50 mM Tris HCl, 50 mM NaCl, 5 mM EDTA, 0.1% SDS, 0.5% deoxycholate, 0.5% Triton X-100 and 0.5% NP-40), which was followed by chromatin shearing using a Fisher Scientific model 500 sonic dismembrator. The samples were then incubated overnight with SureBeads Protein A magnetic beads (Bio-Rad) blocked with salmon sperm DNA (Invitrogen) with the desired antibodies: anti-RELA (Santa Cruz, sc-109X) or anti-NFE2L3 (described above). Normal rabbit IgG (Santa Cruz, sc-2027) and/or input was used as a negative control. After stringent washes, chromatin was eluted in elution buffer (50 mM Tris HCl, 1 mM EDTA and 1% SDS). Eluates were reverse cross-linked overnight at 65°C and deproteinated with Proteinase K for 1 hour at 42-45°C followed by 15 min at 65°C. DNA was extracted and purified via phenol-chloroform-isoamyl alcohol extraction and ethanol precipitation. ChIP-qPCR analyses were performed in a CFX96 Touch Real Time PCR detection system (Bio-Rad) and the following primers were used: NFE2L3 (forward 5′-CCACAGTCATTCACAACGGA-3′ and reverse 5′-GCAGCTGTTCCATACGTTTACA −3′), DUX4 (forward 5′-TCACCTTTGTCATCAGTTCAGG-3′ and reverse 5′-TGATGTAACTC TTGTCTAAGCTCTGC −3′). Fold induction was calculated over IgG. ChIP-seq libraries were prepared according to the NEBNext protocol and sequenced using Illumina HiSeq 2000. For the ChIP-seq analysis, HCT116 cells were treated with TNF (20 ng/ml, 6 hours). Trimming and clipping were performed using Trimmomatic. Reads were trimmed from the 3′ end to have a phred score of at least 30. Illumina sequencing adapters were removed from the reads, and all reads were required to have a length of at least 50 bp. The filtered reads were aligned to *Homo sapiens* assembly hg19. Each readset was aligned using BWA which creates a Binary Alignment Map file (.bam). Quality filtering was then performed using SAMtools (Li et al., 2009). All alignments with MAPQ smaller than 20 and samflag 4 (read unmapped) were excluded. HOMER (Heinz et al., 2010) was used to create QC Tag Directories, to compute ChIP-seq Quality Metrics and to generate BedGraph Track Format files that were loaded in UCSC. Peaks were called using MACS software with default parameters. The peaks called were annotated with HOMER using RefSeq annotations. Gene ontology and genome ontology analyses were also performed at this stage.

Dual-luciferase Reporter Assay

Promoter region was cloned into pGL3 Basic Luciferase Reporter (Promega) by digesting plasmid and annealed primer pair using KpnI-HF® RE-Mix® (R3142S, NEB) and XhoI (R0146S, NEB) and ligating them with T4 DNA ligase (M0202S, NEB). The forward primer was:CCACAACGGATGAAGCATGCATTCTTCCAAGTAACACACAGGTTAAACAAAGAAATGAACAGTTTTTGTAGAATTGAAT GTGTAAACGTAC and the reverse primer was:TCGAGTACGTTTACACATTCAATTCTACAAAAACTGTTCATTTCTTTGTTTAACC

TGTGTGTTACTTGGAAGAATGCATGCTTCATCCGTTGTGGGTAC. The construct was confirmed by DNA sequencing. Aliquots of 5×10^4 293T cells were seeded into 24-well plates. After 24 hours, 250 ng of each independent luciferase reporter plasmid plus 50 ng of pRL-TK (Promega) plasmid as the control were co-transfected with 125 ng, 250 ng or 500 ng of the pCMV4-RELA, or control. Luciferase activity was then measured 24 hours after transfection using the Dual-Luciferase Reporter Assay System with a GloMax Luminometer (Promega). Firefly luciferase activity was normalized to Renilla luciferase activity for each transfected cell sample.

(Co-)Immunoprecipitation

HCT116 cells were transfected with pCMV6-entry-Myc-Flag (PS100001, Origene) or pCMV6-DUX4-Myc-Flag (RC238145, Origene) using X-tremeGene 9 DNA transfection reagent (Roche). Cells were lysed with IP buffer (50 mM Tris-HCl pH 7.9, 1 mM EDTA, 0.1 mM EGTA, 12.5 mM $MgCl_2$, 400 mM NaCl, 20% glycerol, 0.1% SDS, 1% Triton X-100 and a complete-EDTA free protease inhibitor) on ice for 15 min and then sonicated 20 s at the lowest intensity. Cell lysates were clarified by centrifugation at 14,000 rpm for 1 min. Clarified lysates were incubated for 1 hour at 4°C with anti-Flag M2 affinity gel (Sigma, A2220). After three washes with IP buffer, proteins from immunoprecipitations were resolved by SDS polyacrylamide gel electrophoresis (PAGE), visualized by colloidal Coomassie stain and excised from the gel before mass spectrometry analysis. For the co-immunoprecipitation, HCT116 cells were transfected with pCMV-neo-CDK1-HA, pCMV-neo-CDK2-HA, pCMV-neo-CDK4-HA, pCMV-neo-CDK6-HA (Addgene) (van den Heuvel and Harlow, 1993) pCMV6-entry-Myc-Flag and pCMV6-DUX4-Myc-Flag (Origene). For the experiment with DUX4 mutants, HCT116 cells were transfected with pcDNA3.1-Myc, pcDNA3.1-DUX4(WT)-Myc, pcDNA3.1 DUX4(Δ111-131)-Myc, pcDNA3.1 DUX4(Δ141-180)-Myc and pcDNA3.1 DUX4(Δ381-400)-Myc, pcDNA3.1 DUX4(Arg117Ala)-Myc, pcDNA3.1 DUX4(Phe118Ala)-Myc (Genscript), pCMV-neo-CDK1-HA (Addgene) and pCMV-neo-HA (Clontech). Cells were lyzed with IP buffer on ice for 15 min and then sonicated 20 s at the lowest intensity. Cell lysates were clarified by centrifugation at 14,000 rpm for 1 min and were incubated for 2 hours with anti-HA antibody (2 μg/ml of cell lysate, sc-7392, Santa Cruz) followed by 2 hours with protein A and G Sepharose (Millipore) at 4°C. Before immunoprecipitation, protein A and G Sepharose were blocked for 1 hour at 4°C in IP buffer containing 2.5% BSA, 0.16 μg/μl salmon sperm DNA and 0.16 μg/μl *E. coli* tRNA. Then, all immunoprecipitates were washed three times in IP buffer, denatured at 95°C for 10 min and separated on 12% SDS-PAGE for western blot analysis. For endogenous protein immunoprecipitations, HCT116 cells were transduced with shNFE2L3-1. Cells were lyzed with the IP buffer. For each condition, CDK1 antibody (2 μg/ml of cell lysate, sc-54, Santa Cruz) or mouse pre-immune serum (2 μg/ml of cell lysate, sc-2025, Santa Cruz) were incubated for 2 hours at 4°C. Then, we followed the same protocol already described above.

Mass Spectrometry

Destaining was performed in 50% MeOH. Bands were shrinked in 50% acetonitrile (ACN) and reconstituted in 50 mM ammonium bicarbonate with 10 mM TCEP and vortexed for 1 hour at 37°C. Chloroacetamide was added for alkylation to a final concentration of 55 mM. Samples were vortexed for another hour at 37°C. One μg of trypsin was added and the digestion was performed for 8 hours at 37°C. Peptide extraction was conducted with 90% ACN. Extracted peptide samples were dried down and solubilized in ACN 5% formic acid (FA) 0.2%. Samples were loaded on a homemade C18 precolumn (0.3 mm i.d. x 5 mm) connected directly to the switching valve and separated on a homemade reversed-phase column (150 μm i.d. x 150 mm) with a 56 min gradient from 10%–30% acetonitrile (0.2% FA) and a 600 nl/min flow rate on a Ultimate 3000 nano-LC (Dionex) connected to a Q-Exactive Plus (Thermo Fisher Scientific). Each full MS spectrum acquired with a 70,000 resolution was followed by 12 MS/MS spectra, where the 12 most abundant multiply charged ions were selected for MS/MS analysis. Tandem MS experiments were performed using HCD at collision energy of 25%. The data were processed using PEAKS 7.0 (Bio-informatics Solutions) and the human Uniprot database. Tolerances on precursors and fragments were 10 ppm and 0.01 Da, respectively. Variable selected post-translational modifications were carbamidomethyl (C), oxidation (M), deamidation (NQ) and phosphorylation (STY). MS hits were analyzed for enrichment using ReactomePA (Yu and He, 2016).

Prediction of DUX4 Structure using Fold Recognition Domain

Since no crystallographic structure of DUX4 alone is available in the PDB (Protein Data Bank), a model of the protein has been generated based on fold recognition. Sequence of human DUX4 (UniProtKB: Q9UBX2) was obtained from UniProt database (The UniProt Consortium, 2017). DUX4 protein is composed by 424 amino acids for a molecular weight of 44.94 kDa. A model of this protein was build using I-TASSER (a web app designed for 3D structure prediction based on fold recognition) (Roy et al., 2010; Yang et al., 2015; Zhang, 2008).The target sequence has been threaded through a non-redundant PDB structure library by LOMETS (Local Meta-Threading-Server) in order to identify template structures that may have a similar structure or similar structural motif to the query protein. If homologous templates are identified, a template-based fragment assembly procedure (threading, fragment assembly, and iteration) is used to construct full-length models. The outputs of the I-TASSER modeling contain the top 5 models predicted for the query sequence. Each model is associated to C-score and TM-score. C-score is a confidence score for estimating the quality of predicted models. TM-score reflects the structural similarity between two structures taking into account RMSD (Root-Mean-Square Deviation) between two atoms or residues. RMSD is sensitive to local error, including misorientation of side chains, tails, and random coils, which can increase RMSD values while the global topology is correct. A correction is applied to minimize the effect of local errors. Top 5 predicted models show two groups of structure regarding to general topology, C-score (model with a high confidence) and TM-score (high similarity with structures present in the PDB). The first group contains 3 of the 5 predicted models with

very similar structure and high scores. A structure superposition confirmed that these 3 models are very close to each other with slight changes in the random coils region. The second group is less relevant with low scores and a poor recovery with PDB templates. A predicted model with higher C-score value and TM-score value (model 3) was kept for further investigation.

Modeling DUX4-CDK1 Complex

Based on biological evidence, a model of DUX4-CDK1 complex has been built using ZDOCK 3.0.2. (Mintseris et al., 2007; Pierce et al., 2011). This software studies all possible binding modes by translation and rotation of each protein. We carried out this evaluation by using an energy-based scoring function called IFACE. The score depends on statistical potential, shape complementarity, electrostatic, and an experimental unbound protein benchmark. To start the modeling, we searched a similar complex to the one studied in the PDB. We found a comparable structure, the complex of CDK1-Cyclin B1-CKS2 with a small molecule named NU6102 (PDB: 5LQF) (Coxon et al., 2017). In order to validate the docking, each protein from structure 5LQF was individualized in a file (CDK1, Cyclin B1 and CKS2). Each protein was structurally prepared using Biovia Discovery Studio 2016. The three proteins were docked together using ZDOCK and the result show an identical overlay with the complex present in the PDB (slight changes in random coils regions). The second step consists in the creation of the query complex. For this, the 3D model of DUX4 was used as input in ZDOCK with CDK1 and Cyclin B1. The complex with the highest ZDOCK-score shows identical protein-protein interactions (PPIs) between CDK1 and Cyclin B1 and a complete overlay for these two proteins compared to the reference structure 5LQF. DUX4 has been shown to interact with CDK1 at the same regions as CKS2 with similar interactions (hydrophobic at the core of the surface interaction and electrostatic at the borders).

In Vitro Protein Interaction (GST Pull-down Assay)

Recombinant DUX4-Myc-FLAG was produced in HEK293 cells transiently transfected using the calcium phosphate method with 15 μg (10 cm) of pCMV6-DUX4-Myc-FLAG and then immunoprecipitated with anti-FLAG M2 Affinity Gel (Sigma-Aldrich), washed three times for 5 min in 1X TBS, eluted for 1 hour at 4°C with 250 ng/μl of FLAG peptide (Sigma-Aldrich) in 1X TBS and protein concentration was evaluated using a NanoDrop2000c spectrophotometer (A280). *In vitro* protein interactions were performed as previously described (Lessard et al., 2018). GST (100 ng according to company; SRP5348, Sigma-Aldrich) or GST tagged human active CDK1/cyclin B1 (300 ng according to company; SRP5009, Sigma-Aldrich) or GST tagged human CDK1 (300 ng according to company; C22-14G, Signal Chem) were incubated with human recombinant DUX4-Myc-FLAG (200 ng) in 300 μL of PB buffer (20 mM HEPES, pH 7.5, 130 mM KCl, 5 mM $MgCl_2$, 1 mM DTT, 0.5 mM EDTA, 0.05% NP40) and mixed using a rotating machine at 30°C for 2 hours. Proper amounts of glutathione-Sepharose beads (17-0756-01, GE Healthcare) were washed three times with PB buffer. Then, 10 μL of glutathione beads and 5 μL of BSA (25% stock solution) were added to proteins mix and incubation continued at room temperature for 30 min with rotation. The beads were then washed three times for 15 minutes with PB buffer at room temperature with rotation. Then, the appropriated quantity of 6X loading buffer (0.5 M Tris-HCl pH 6.8, 30% glycerol, 10% SDS, 1% bromophenol blue and 15% β-mercaptoethanol) was added. The samples were boiled for 5 min and separated by SDS-PAGE for western blotting.

Purification of GST-DUX4

Plasmid coding for human DUX4 (pGEX-6-p1, N-term GST-HRV 3V protease cleavage site) was a gift from Professor Scott Harper (Nationwide Children's Hospital, USA). The plasmid (10 ng) was transformed into the bacterial strain *E. coli* BL21 (DE3). The transformed cells were plated on LB plates containing ampicillin (100 μg/ml) and incubated overnight at 37°C. One colony was picked from one of the plates and used to inoculate 5 mL of LB broth containing 100 μg/ml ampicillin. The culture was grown overnight at 37°C with shaking at 250 rpm. A bacterial stab was prepared by adding 150 μL of cell culture to 850 μL of glycerol 50% (sterile). Aliquots were kept at −80°C. Preculture (x2) was prepared by inoculating 250 μL of bacterial stock to 5 mL of TB medium (yeast extract 24 g/L, tryptone 20 g/L, glycerol 0.4% (V/V), 0.017 M KH_2PO_4 and 0.072 M K_2HPO_4) with ampicillin 100 μg/mL. Culture was grown overnight at 37°C with shaking. For production of GST-fusion protein, culture was divided into equal amounts between four flasks containing 250 mL TB/Amp medium and allowed to grow at 37°C to A_{600} = 0.6. The culture was induced with 0.1 mM isopropyl β-D-1-thiogalactopyranoside (IPTG) and growth was continued overnight at 20°C with agitation. Induced culture was centrifuged at 6000 x g for 20 min. Cell pellet was resuspended in 60 mL of Lysis buffer (50 mM Tris-HCl pH 8.0, 150 mM NaCl, 0.1 mM EDTA, 0.1% Triton X-100, 1 mM DTT, RNase and protease inhibitor cocktail (Complete, 1 tablet for 50 mL of solution, Roche). Cells were lysed on ice by sonication using a cell disrupter. Crude extract was centrifuged at 9000 rpm for 45 min at 4°C to recover the lysate. The supernatant was filtered through 0.45 μm and 0.2 μm filters. Proteins lysate was loaded onto a 1 mL GSTrap FF (GE Healthcare) equilibrated with 50 mM Tris-HCl pH 8.0, 400 mM NaCl, 0.1 mM EDTA, 1 mM DTT and 5% glycerol. The charged column was washed with the equilibration buffer until a stable baseline was attained. Target protein was eluted with elution buffer (50 mM Tris-HCl pH 8.0, 400 mM NaCl, 0.1 mM EDTA, 1 mM DTT, 5% glycerol and 10 mM reduced gluthatione). After elution, appropriate fractions were pooled and the buffer was changed (50 mM Tris-HCl pH8.0, 150 mM NaCl, 0.1 mM EDTA, 1 mM DTT and 5% glycerol) using PD-10 desalting column (GE Healthcare). Protein concentration was determined using NanoDrop and flash freeze in liquid nitrogen for storage (−80°C) until use.

Microscale Thermophoresis (MST)

MST measurements were performed on a Nanotemper Monolith NT.115 instrument (Nano- temper Technologies, GmbH) using His-tag fluorescent labeling. Recombinant human CDK-1 protein (187447, Abcam) purified to homogeneity, was freshly labeled with the Monolith His-Tag RED-tris-NTA labeling dye (2nd generation) according to the supplied protocol (Nanotemper Technologies, GmbH). Measurements were performed in PBS pH 7.4 containing 2.5% glycerol, 5 mM GSH, 0.5 mM DTT and 0.05% Tween-20 in standard treated capillaries (MO-K022, Nanotemper Technologies, GmbH). The final concentrations of CDK-1 in the assay were 50 nM. DUX-4 was then titrated in 1:1 dilutions following manufacturer's recommendations. GST protein (SRP5348, Sigma) was used as negative control. All reactions medium underwent brief centrifugation at room temperature followed by 5 min incubation at 25°C after loading into capillaries. Measurements were performed at 25°C in triplicates using 40% LED power and medium MST power, LaserOn time was 20 s, Laser Off time 3 s.

Kinase Assay

HCT116 cells were transduced with a combination of vectors driving non-silencing controls (NTC shRNA or pLV scramble), shNFE2L3-1 or shDUX4. The same number of cells was lyzed in the same volume of IP buffer for each condition. Lysates were incubated for 2 hours at 4°C with antibody against CDK1 (2 mg/ml, sc-54, Santa Cruz). For the kinase assay, we used the same protocol described above for the co-immunoprecipitation but subsequently, immunoprecipitates were washed three times in kinase buffer (9802, Cell Signaling) and then incubated at 30°C for 30 min with 40 μl of kinase buffer containing 200 mM ATP (9804, Cell Signaling) and 2 μg of recombinant human Histone H1 (His tag N terminus) protein (198676, Abcam). Finally, reactions were stopped by heating at 95°C for 10 min and separated on 12% SDS-PAGE for western blot analysis.

QUANTIFICATION AND STATISTICAL ANALYSIS

Statistical Methods

All data are shown as mean values ± standard error of the mean (SEM) unless indicated otherwise. Sample numbers of data obtained from animal experiments refer to the number of individual mice, as specified in the figure legends. Statistical analysis (two-tailed Student's t test) was performed using Excel and Mann–Whitney U test was performed using Statistica software (StatSoft, Tulsa, OK), as indicated in the figure legends. A value of $p < 0.05$ was considered statistically significant.

DATA AND CODE AVAILABILITY

ChIP-seq Data Link

https://onedrive.live.com/redir?resid=3F5A1FD25439B0CE!108&authkey=!APH0PPlEs_4AqUw&ithint=folder%2c.

TMA Link

https://onedrive.live.com/redir?resid=3F5A1FD25439B0CE!109&authkey=!ACVMRj5FWUvVPZg.

Cell Reports, Volume *29*

Supplemental Information

NFE2L3 Controls Colon Cancer Cell Growth through Regulation of DUX4, a CDK1 Inhibitor

Marina Bury, Benjamin Le Calvé, Frédéric Lessard, Thomas Dal Maso, James Saliba, Carine Michiels, Gerardo Ferbeyre, and Volker Blank

Figure S1

A

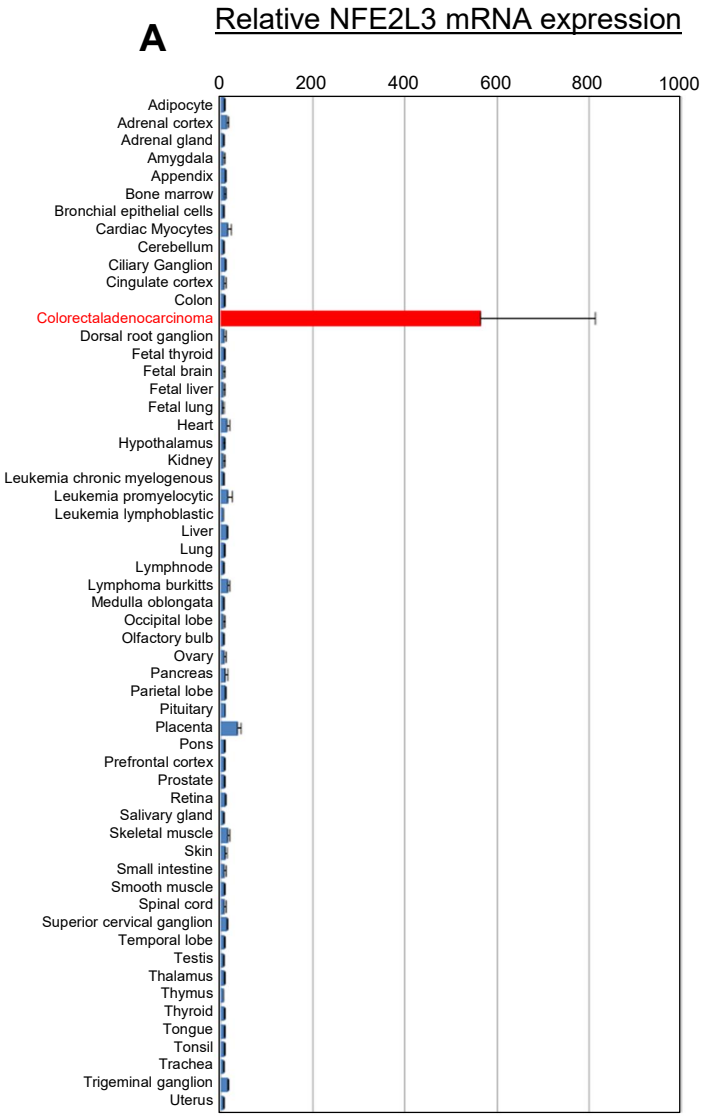

B

Analysis type by cancer	Cancer vs. Normal	
Bladder Cancer		
Brain and CNS Cancer		
Breast Cancer	2	
Cervical Cancer		
Colorectal Cancer	17	
Esophageal Cancer		
Gastric Cancer	1	
Head and Neck Cancer		
Kidney Cancer		
Leukemia		
Liver Cancer		
Lung Cancer		
Lymphoma	4	
Melanoma		
Myeloma		
Other Cancer	3	
Ovarian Cancer	1	
Pancreatic Cancer		
Prostate Cancer		
Sarcoma		

Threshold (p-value): 10^{-5}
Threshold (fold change): 4
Threshold (gene rank): Top 10%

C

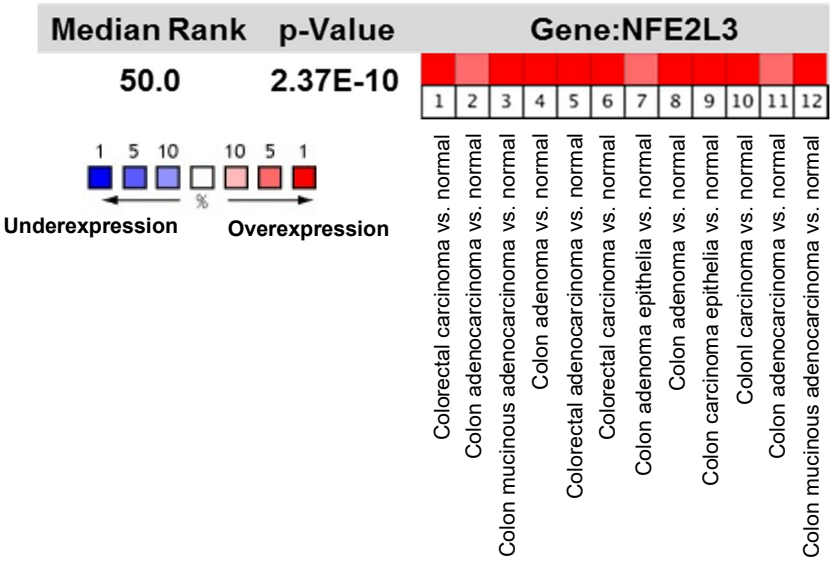

Figure S1: NFE2L3 upregulation in colon cancer, related to Figure 1. (A) Bar graph presenting *z*-scores of relative microarray expression of NFE2L3 in various human tissue samples. Data collected from www.biogps.org (McCall et al., 2011; Wu et al., 2009). Error bars represent the median absolute deviation. (B) NFE2L3 expression in multiple cancer microarray data sets available in Oncomine (Rhodes et al., 2004). (C) The median NFE2L3 rank was assessed across 12 analyses comparing the normal tissue group to each colorectal cancer data sets. The p-value is given for the median-ranked analysis (www.oncomine.org).

Figure S2

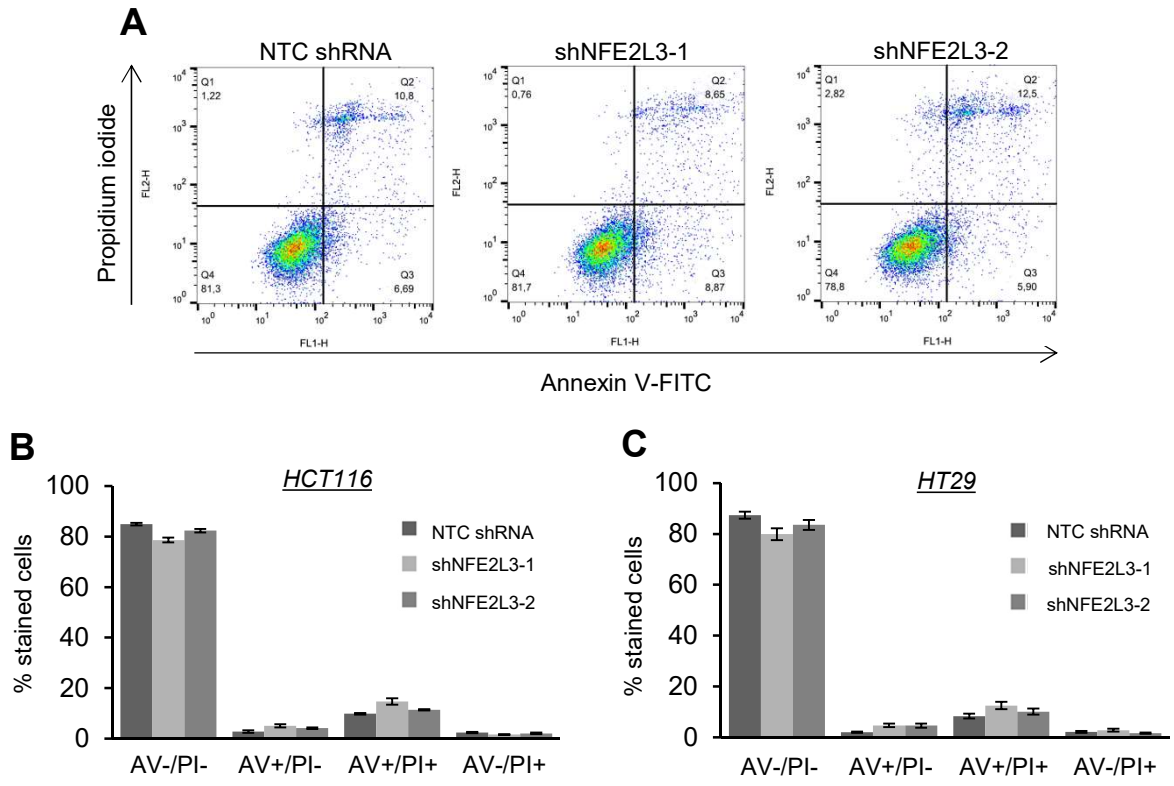

Figure S2: NFE2L3 knockdown does not induce apoptosis, related to Figure 2. (A) Comparison of flow cytometry histograms of Annexin V and propidium iodide stained HCT116 cells transduced with a NTC shRNA or NFE2L3-specific shRNAs (shNFE2L3-1 or -2). (B, C) Annexin V/PI based apoptosis analysis in NTC shRNA or NFE2L3-specific shRNAs (shNFE2L3-1 or -2) transduced HCT116 and HT29 cells. Error bars are means ± SEM, $n = 3$ independent experiments.

Figure S3

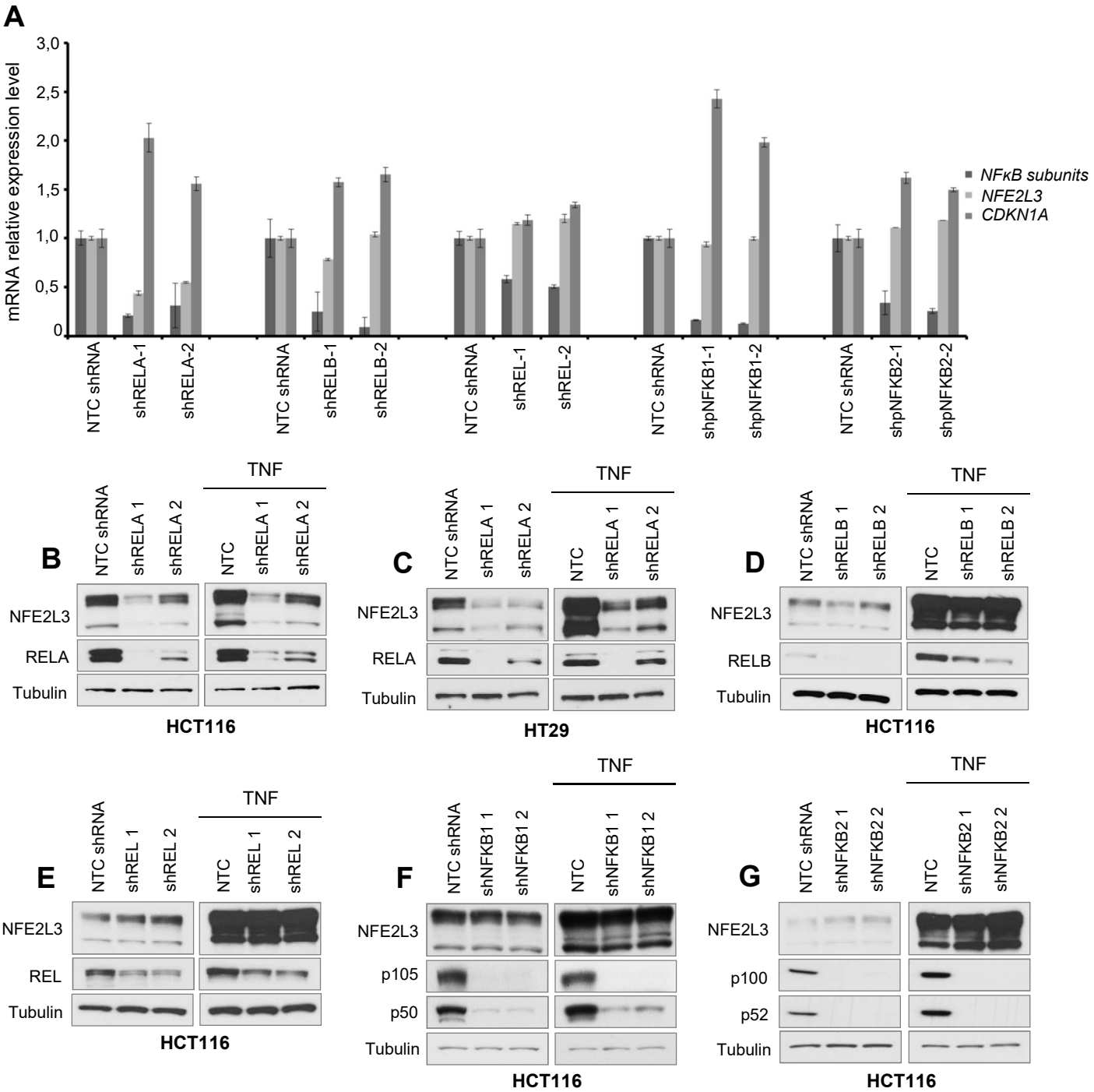
A
mRNA relative expression level
3,0
2,5
2,0
1,5
1,0
0,5
0
NFκB subunits
NFE2L3
CDKN1A
NTC shRNA
shRELA-1
shRELA-2
NTC shRNA
shRELB-1
shRELB-2
NTC shRNA
shREL-1
shREL-2
NTC shRNA
shpNFKB1-1
shpNFKB1-2
NTC shRNA
shpNFKB2-1
shpNFKB2-2
B
TNF
NTC shRNA
shRELA 1
shRELA 2
NTC
shRELA 1
shRELA 2
NFE2L3
RELA
Tubulin
HCT116
C
TNF
NTC shRNA
shRELA 1
shRELA 2
NTC
shRELA 1
shRELA 2
NFE2L3
RELA
Tubulin
HT29
D
TNF
NTC shRNA
shRELB 1
shRELB 2
NTC
shRELB 1
shRELB 2
NFE2L3
RELB
Tubulin
HCT116
E
TNF
NTC shRNA
shREL 1
shREL 2
NTC
shREL 1
shREL 2
NFE2L3
REL
Tubulin
HCT116
F
TNF
NTC shRNA
shNFKB1 1
shNFKB1 2
NTC
shNFKB1 1
shNFKB1 2
NFE2L3
p105
p50
Tubulin
HCT116
G
TNF
NTC shRNA
shNFKB2 1
shNFKB2 2
NTC
shNFKB2 1
shNFKB2 2
NFE2L3
p100
p52
Tubulin
HCT116

Figure S3: NFE2L3 is principally regulated by the RELA subunit of NF-κB, related to Figure 3. (A) Quantitative reverse transcription PCR analysis of transcripts of NF-κB family members, NFE2L3 and CDKN1A (p21) in HCT116 cells transduced with a NTC shRNA, or RELA-specific shRNAs (shRELA-1 or -2), or RELB-specific shRNAs (shRELB-1 or -2), or REL-specific shRNAs (shREL-1 or -2), or NFKB1-specific shRNAs (shNFKB1-1 or -2) or NFKB2-specific shRNAs (shNFKB2-1 or -2) (mean ± SD). (B, C) Immunoblot analysis of NFE2L3 in HCT116 and HT29 cells transduced with a NTC shRNA or RELA-specific shRNAs (shRELA-1 or -2) untreated or treated with TNF (20 ng/ml, 6 hours). (D-G) Immunoblot analysis of NFE2L3 in HCT116 cells transduced with a NTC shRNA or RELB-specific shRNAs (shRELB-1 or -2) (D), or REL-specific shRNAs (shREL-1 or -2) (E), or NFKB1-specific shRNAs (shNFKB1-1 or -2) (F), or NFKB2-specific shRNAs (shNFKB2-1 or -2) (G) untreated or treated with TNF (20 ng/ml, 6 hours).

Figure S4

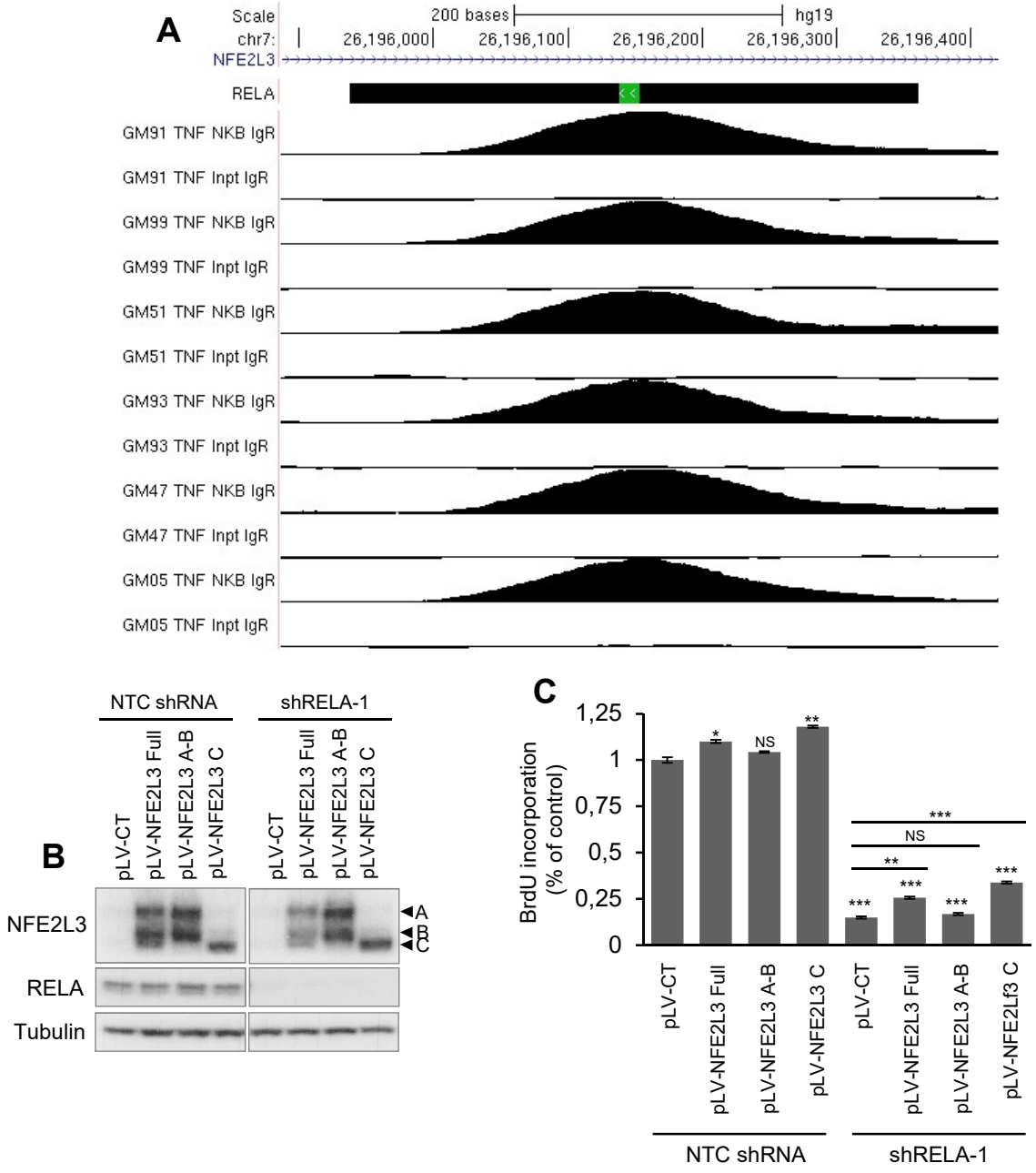

Figure S4: NFE2L3 is implicated in the phenotype of RELA knockdown cell line, related to Figure 3. (A) ChIP-seq data from the ENCODE project consortium showing RELA occupancy over promoter regions of NFE2L3 was extracted from the UCSC genome browser; ChIP-seq data from various tissues and cells; Input is shown for reference. (B) Immunoblot analysis of HCT116 cells transduced with a NTC shRNA or RELA-specific shRNA (shRELA-1) upon reexpression of the different forms of NFE2L3 (see Figure 2C for description of A, B or C form). (C) BrdU incorporation in HCT116 cells an in (B) assessed by ELISA. Error bars are mean ± SEM, $n = 3$ independent experiments, $^{*}p<0.05$, $^{**}p<0.01$, $^{***}p<0.001$, NS = not significant, two-sided Student's *t*-test.

Figure S5

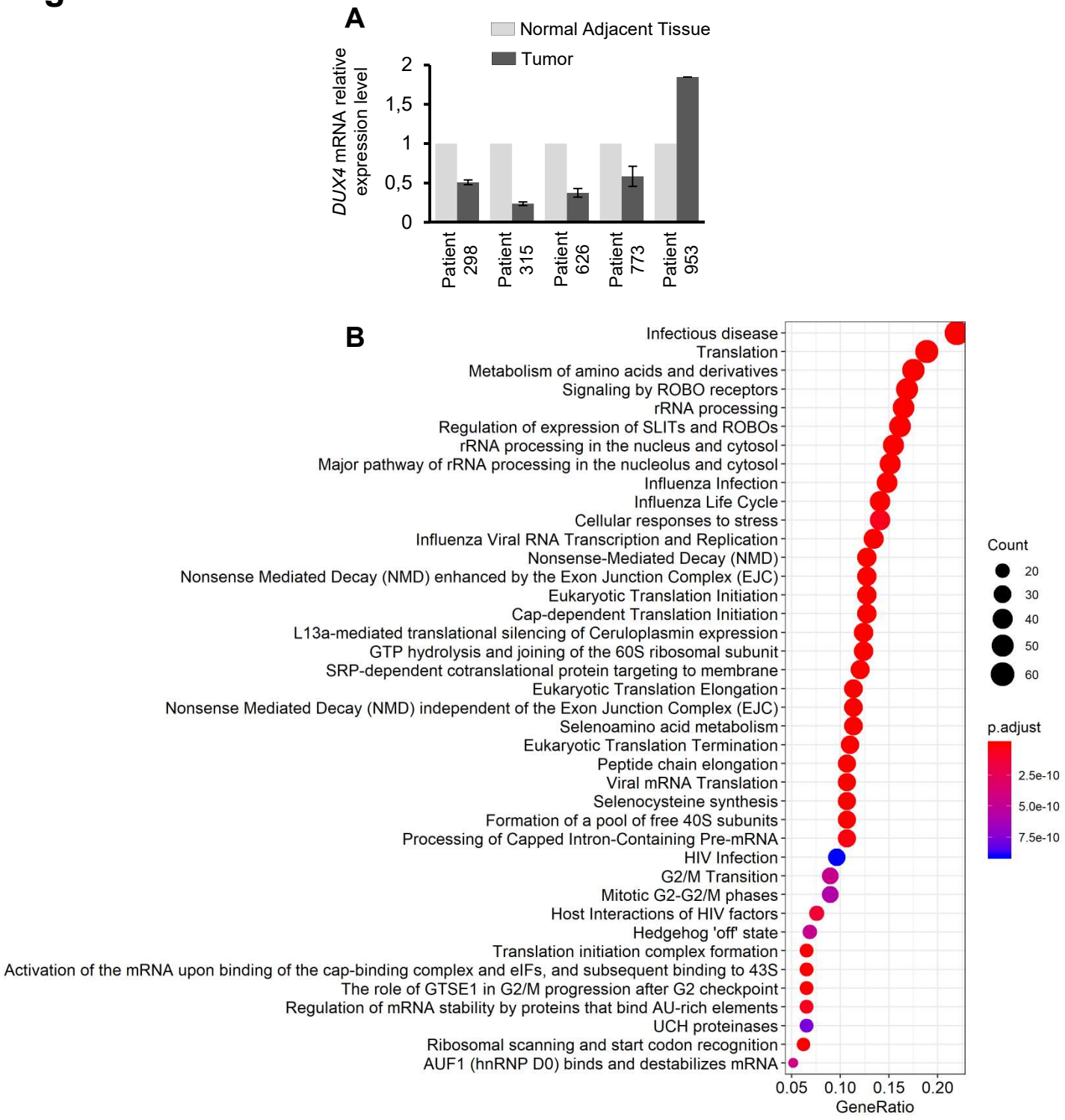

Figure S5: DUX4 expression in patient samples and pathway enrichment analysis of DUX4 protein IP , related to Figures 1, 4 and 5. (A) *DUX4* mRNA expression in colon cancer and adjacent normal tissue of five different colon adenocarcinoma patients (mean ± SD) as analyzed by quantitative reverse transcription PCR analysis. See Figure 1B for comparison with *NFE2L3* mRNA expression in the same patient tissue samples. (B) Dotplot of the top 40 pathways enriched among DUX4 immunoprecipitated proteins. Data was analyzed using ReactomePA with a qvalue cutoff of 0.05 calculated using the Benjamini-Hochberg procedure.

Figure S6

A

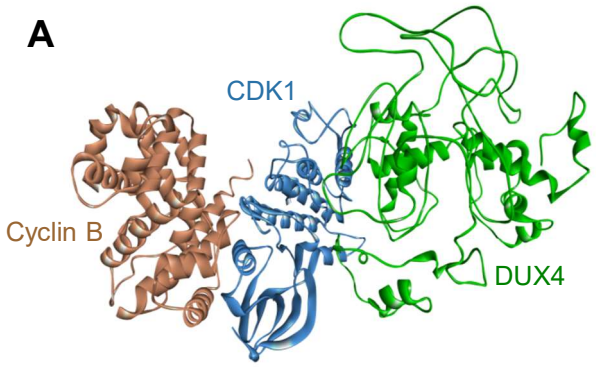

B

CDK1 residues	DUX4 residues	Type	Distance (Å)	Angle XDA	Angle DAY
ASP207	ARG117	Electrostatic	5.55393		
ASP211	ARG146	Electrostatic	4.47743		
ASP207	ARG146	Electrostatic	3.46249		
VAL165	LEU391	Hydrogen Bond	3.08399	57.029	135.751
ASP207	ARG117	Hydrogen Bond	3.37782	48.206	148.913
SER208	ARG117	Hydrogen Bond	2.53617	13.547	70.749
ASP211	ARG146	Hydrogen Bond	3.49703	25.573	134.91
TRP168	ALA395	Van der Waals	3.65716		
LYS88	PRO396	Van der Waals	5.495		
ILE210	ALA174	Van der Waals	3.68044		
TRP168	ALA395	Van der Waals	4.1564		
TRP168	PRO396	Van der Waals	4.70076		
HIS205	PRO150	Van der Waals	4.8042		
TRP244	ALA167	Van der Waals	4.65777		
ARG215	PHE118	Van der Waals	4.43078		

C

Uniprot accession Number	Name	10	20	30	40	50	60
P06493	CDK1_HUMAN	---------MEDYTKIEKIGEGTYGVVYKGRHKTTGQVVALKKIRLESEEEGVPSTIREISLLKELNHPNIVKLLDVIHTENKLYLVFEFLSMDLKKYLDSIPPGQYMDSSLVKSYLYQILQGIVFCHSRRVLHRDLKPQNLLIDDKGTIKLADFGLARAFGIPIRVYTHEVVTLWYRSPEVLLGSARYSTPVDIWSIGTIFAEMATKKPLFHGDSEIDQLFRIFRTLGTPDEVVWPGVTSMPDYKPSFPKWARQDFSKVVPPLDEDGRSLLSQMLHYDPNKRISAKAALAHPFFQDVTKPVPHLRL
P24941	CDK2_HUMAN	---------MENFQKVEKIGEGTYGVVYKARNKLTGEVVALKKIRLDTETEGVPSTAIREISLLKELKHPNIVRLHDVIHSEKRLTLVFEFLHQDLKKFMDASALTGI
P11802	CDK4_HUMAN	---------MATSRYEPVAEIGVGAYGTVYKARDPHSGHFVALKSVRVPNGGGGGGGLPISTVREVALLRRLEAFEHPNVVRLMDVCATSRTDREIKVTLVFEHVDQDLRTYLDKAPPPGLPAETIKDLMRQFLRGLDFLHANCIVHRDLKPENILVTSGGTVKLADFGLARIYSYQMALTPVVVTLWYRAPEVLLQSTYATPVDMWSVGCIFAEMFRRKPLFCGNSEADQLGKIFDLIGLPPEDDWPRDVSLPRGAFPPRGPRSVQSVVPEMEESGAQLLLEMLTFNPHKRISAFRALQHSYLHKDEGNPE
Q00534	CDK6_HUMAN	MEKDGLCRADQQYECVAEIGEGAYGKVFKARDLKNGGRFVALKRVRVQTGEEGMPLSTIREVALLKRLEAFDHPNVVRLFDVCTVSRTDRETKLTLVFEHVDQDLTTYLDKVPEPGVPTETIKDMMFQLLRGLDFCHSHRVLHRDLKPQNILVTSSGQIKLADFGLARIYSFQMALTSVVVTLWYRAPEVLLQSSYATPVDLWSVGCIFAEMFRRKPLFRGSSDVDQLGKILDVIGLPGEEDWPRDVALPRQAFHSKSAQPIEKFVTDIDELGKDLLLKCLTFNPAKRISAYSALSHPYFQDLERCKENLDSHLPPSQNTSELNTA

Figure S6: Potential DUX4-CDK1 interactions and comparison with the other CDK family members, related to Figure 5. (A) Representation of the ternary complex of DUX4-CDK1-Cyclin B1 by using ZDOCK software with the highest C- and TM-scores. (B) Summary of amino acids and type of bonds implicated in the interaction between DUX4 and CDK1. (C) Sequence alignment of the different human CDKs: CDK1 (Uniprot accession number P06493), CDK2 (P24941), CDK4 (11802) and CDK6 (Q00534) based on the EMBL-EBI algorithm MUSCLE. The most conserved residues are highlighted in red and the residues that interact with DUX4 are highlighted in green (based on ternary complex described in Figure S6A). Orange highlights the amino acids in CDK2, CDK4 and CDK6 at the same position as the DUX4-CDK1 interacting residues.

Table S2

Real-time PCR primers		
Name	5' forward primer (5'-3')	3' reverse primer (5'-3')
NFE2L3	TCAGCAGAATGATGATGATGAAA	TGTCCCATTCAGATGTCTCTCA
MKI67	AGAAGACAGTACCGCAGATGA	CGGCTCACTAATTTAACGCTGG
DUX4	GCGGAGAACTGCCATTCTTTT	TCCAGGTTTGCCTAGACAGC
RELA	TCATGAAGAAGAGCTCCTTTCAGC	CTGGCTTGGGGACAGAAG
RELB	GCTCTACTTGCTCTGCGACA	GGCCTGGGAGAAGTCAGC
REL	TGAACATGGTAATTTGACGACTG	ACACGACAAATCCTTAATTCTGC
NFKB1	CCTGGAACCACGCCTCTA	GGCTCATATGGTTTCCCATTTA
NFKB2	ACACCGTTGTACAAAGATACGC	GGCCCGGCTCTGTCTAGT
ACTINB	CCCAACGCACCGAATAGTTACG	GCTGCCCATCATCATGACCT
GAPDH	TCCCACAGCTGGTACCAATAGGA	TCCTGTGGCATGTTTTTGAATCTC
CDKN1A	ACCCTTGTGCCTCGCTCAGG	GCGTTTGGAGTGGTAGAAATCTGT

Table S2, related to STAR Methods: Sequence of qPCR primers